Photovoltaic Performance of P_3HT:CNT:PCBM based Bilayer Solar Cell

Submitted by

MD. Tahmidul Islam (11210001)

Saurav Kumar Mondal (11210003)

A Thesis

Submitted as the Partial Fulfillment for the Degree of

Bachelor of Science in Electrical and Electronic Engineering

Department of Electrical and Electronic Engineering

BRAC University

Dhaka-1212, Bangladesh

CERTIFICATE OF APPROVAL

The thesis entitled **"Photovoltaic Performance of P_3HT:CNT:PCBM based Bilayer Solar Cell"** submitted by **MD. Tahmidul Islam, Saurav Kumar Mondal** has been accepted satisfactory in partial fulfillment of the requirement for the degree of Bachelor of Science in Electrical and Electronics Engineers on April, 2016

Supervisor

_____

(Dr. Sharif Mohammad Mominuzzaman)
Professor
Department of Electrical and Electronic Engineering
Bangladesh University of Engineering and Technology (BUET)

CANDIDATE DECLARATION

It is hereby declared that this thesis or any part of it has not been submitted elsewhere for the award of any degree or diploma.

Author

_____

MD. Tahmidul Islam

Author

_____

Saurav Kumar Mondal

ACKNOWLEDGEMENT

We are grateful to the Almighty for directing us toward the right path in order to pursue the requirement of the full thesis work.

There are some people we would like to thank who have helped us in our research. First and foremost we would like to express our gratitude towards our respected thesis supervisor, **Dr. Sharif Mohammad Mominuzzaman,** Professor of EEE department BUET, for his insight and direction. His faith in us and motivation has provided us with the confidence to achieve our goals.

We would also like to thank **Saad Mohammad Khan** who helped in our research and always believed in our abilities.

Lastly, we are ever grateful to our Parents and well-wishers for supporting and encouraging us throughout the work.

TABLE CONTENTS

LIST OF FIGURES

LIST OF TABLE

Abbreviations

OSC	**Organic Solar Cells**
OPV	**Organic Photovoltaic**
BHJ	**Bulk Hetero Junction**
J_{sc}	**Short Current Density**
V_{oc}	**Open circuit Voltage**
FF	**Fill Factor**
PCE	**Power Conversion Efficiency**
CNT	**Carbon Nanotube**
P_3HT	**Poly (3-hexylthiophene)**
PCBM (6,6)	**Phenyl C61 Butyric acid Methyl ester**
HOMO	**Highest Occupied Molecular Orbital**
LUMO	**Lowest Unoccupied Molecular Orbital**

ABSTRACT

Organicbilayer solarcells have the potential to replace silicon based solar cell devices due to its low cost fabrication cost and high mechanical flexibility. However, despite possessing such remarkable properties their application in the main stream market hasn't beenfeasible enough due to its low PCE. The efficiency of bilayer heterojunction solar cell is limited mainly due to the low hole mobility of the polymer and the low UV region absorptivity of the active composite. The primary reason for the low PCE of bilayer organic solar cell is its low carrier mobility which is hindered by the hopping transport mechanism of the organic active layer.CNTs are known to have high carrier mobility due its ballistic property and can also absorb photon wavelengths in the infra-red region. This exciting optical and electrical property of CNTs makes them a promising material as an additive to Polymer: Fullerene based bilayer OSCs. In this thesis we examine the impact of CNT on the J-V characteristics of P_3HT: PCBM based bilayerheterojunction solar cell. The optical and electrical simulationof the bilayerheterojunction solar cell was carried out using the simulation tool OPV lab which uses the optical transfer matrix methodology to determine the optical properties of the organic active layer. The tool also numerically solves the 1D drift-diffusion equation to predict the J-V characteristics of the organic photovoltaic deviceThe result obtained from the J-V curve show that the photovoltaic performance of the P3HT:PCBM solar cell devices depend on the concentration of CNT. The incorporation of the 1% CNT improved the J_{sc} by 10%. The V_{oc} at 1weight percentageCNT remained relatively same as the reference devices while the power conversion efficiency enhanced by 34%

1. Motivation and Outline

1.1 The Background

1.1.1 Limited Fossil Fuels and Environmental Impact

At present time we are vigorously reliant on fossil fuel, for example, coal, oil, normal gas and wood for our day by day need of vitality prerequisites. In 2011, fossil fuel contributed roughly 82% of world's essential vitality use (Source: Energy Information Agency). These wellsprings of vitality have a constrained supply including Uranium and are non-renewable.

In light of the world's populace development slant, an aggregate populace of nine billion in the following 50 a long time and 10 billion by year 2100 has been anticipated. The world's vitality interest will increment in any event proportionately. A proceeding with ascend in oil costs is relied upon because of expanding interest. As indicated by the US division of vitality, fossil energizes will be generally devoured inside of 100-120 a long time. A couple of different assessments say it will be drained even before the end of this century. In any case, these assessed times are not very a long ways ahead before we may confront an incredible emergency of vitality supply. Along these lines, we have to search for enduring or renewable wellsprings of vitality.

People are including more than 30 billion metric tons (30^{12}Kg) of CO_2 to the air each year, principally by blazing fossil fuel. Uncontrolled deforestation exacerbates things because of the failure of plants to handle the quick inundation of CO_2, coming about a dangerous atmospheric devation. The worldwide mean surface temperature has officially expanded by 0.3-0.6℃ since the late nineteenth century and the worldwide ocean level has expanded by 10-25cm [1]. With the present CO_2 emanation situation a temperature increment of 0.6-7℃ by 2010 is extrapolated. Unquestionably this will have a staggering impact on human life in coming decades.

In such conditions, advancement of option wellsprings of environmentally friendly power vitality, for example, hydro-power, wind power, tidal force and sun oriented force get to be inescapable.

1.1.2 Renewable Sources of Energy

We have plentiful free vitality sources like wind, tsunamis, daylight, water repository potential and so on. One of our objectives in gathering vitality from these sources ought to be less hurtful to people what's more, the earth. Also, the life-time vitality yield quality ought to be significantly more than its information costs in establishment, manufacture, work, innovative work, support and so on. At the end of the day, the higher the vitality payback values the better.

1.1.2.1 Wind Power

Wind vitality has been utilized for eras and is as a part of bottomless supply. This vitality is changed over into other valuable type of vitality, e.g. wind turbines for producing power, windmills for mechanical energy to machines, wind pumps for pumping water, sails to push ships and so forth. Sailboats and cruising ships have been generally utilized for a huge number of years. The principal commonsense windmill was utilized some place somewhere around seventh and ninth century in Iran [2]. In late innovation, wind vitality is for the most part used to drive turbines to create power which is either put away utilizing batteries or specifically encouraged to the force network. Developing interest for wind power era in the business sector is because of its spotless, bounteous supply and one of the least expensive renewable vitality regarding vitality payback esteem. US Branch of Vitality has assessed that wind force could contribute up to 20% of the country's aggregate power supply by 2030. All out wind vitality creation today is, notwithstanding, under 4% of overall power use however the yearly development as of late is more than 25%, as indicated by World Wind Vitality Affiliation WWEA 2011 report [3]. American Wind Vitality Affiliation 2011 report says that wind vitality cost has gone down to 5-6 pennies/kWh which is 2 pennies less expensive than coal-based power era.

1.1.2.2 Hydro Power

Hydro control additionally has been utilized from old times for driving watermills, material plants and so on. The force is gotten from the motor vitality of the water momentum or falling water from a dam or supply. The idea is like wind force era yet since water is much denser than air, it can create impressive force with even a moderate water stream. Electric generators

presented in the mid twentieth century could be combined with hydro turbines to produce power. From that point forward there has been a colossal ascent in hydroelectric force plant set up everywhere throughout the world. It is the most broadly utilized type of renewable vitality, meeting 16% of overall vitality need in 2010[4].

The expense of hydroelectricity for plants bigger than 10MW is around 3 to 5 US pennies/kWh making it the least expensive renewable vitality and tantamount to vitality delivered from fossil energizes [4]. It is additionally considered to have the minimum natural effect as far as contamination and transfer of the waste items.

Tsunamis and streams are likewise used to produce power by utilizing potential vitality of the water head made by low and high sea tides. The dynamic vitality of the tidal streams is too used to drive the water turbines. Tidal force is additionally a type of hydro power and is renewable vitality source. These are profoundly unsurprising contrasted with wind vitality and daylight.

1.1.2.3 Solar Energy

Our planet gets ~1.2^{17} watts power from the sun though the current overall electric vitality utilization is ~10,000 times littler, i.e. ~1.3^{13} watts [5]. Meaning, the earth gets more vitality in an hour than the overall vitality requirement for the entire year. Sunlight based cells on the other hand photovoltaic cells straightforwardly change over sunlight based vitality as enthusiastic photons into power. Photovoltaic commercial enterprises are as yet battling with the way that the vitality payback esteem for sunlight based vitality framework is much higher contrasted with that of fossil fills. We have to concentrate more on innovative work for expanding photovoltaic proficiency and life-time and for diminishing creation costs by investigating elective less expensive semiconducting dynamic materials and so forth.

1.1.3 Photovoltaic Technology and Development

Worldwide enthusiasm for photovoltaic (PV) innovation has expanded strongly in the course of the most recent decade because of hypothesis on the likelihood of a future vitality emergency,

contamination, improvements in creation innovation and so on. Staggering additions in both the PV market and in exploration movement are seen. A sunlight based cell or photovoltaic cell specifically changes over the daylight into power. The primary sunlight based cell was developed by Charles Fritts in 1880s where he utilized Selenium semiconductor and a meager layer of gold. The semiconductor served as photon safeguard and the electron-opening pair is isolated by the electric field in the Au-Se Schottky intersection. The main silicon sunlight based cell where electron-opening sets were isolated at the p-n intersection was created by Russel Ohl in 1941. The cell was amazingly enhanced by Gerald Pearson, Calvin Fuller and Daryl Chapin in 1954 at Ringer Research facility and was equipped for 6% transformation proficiency from direct daylight [6].

Somewhere around 1970 and 1983 photovoltaic establishments became quickly, however falling oil costs in the early 1980s frustrated the development in PV research from 1984 to 1996. Since 1997, PV improvement has quickened because of supply issues with oil and characteristic gas, an unnatural weather change concerns, and the enhancing financial position of PV in respect to other vitality advances [7]. Photovoltaic generation development has arrived at the midpoint of 40% every year since 2000. As indicated by the European Photovoltaic Industry Affiliation the world's aggregate introduced limit achieved 40 GW in 2010 from 23 GW in 2009.

Right now, the greater part of the sun powered cells are made of silicon where expenses are high, numerous option sorts of sun based cells are created and new less expensive materials have been researched to supplant silicon. The utilization of undefined silicon is one of its answers as it is less costly and higher light retaining capacity contrasted with monocrystalline or polycrystalline silicon. As of late, natural sun based cells (OSCs) having much less expensive photograph dynamic layer natural semiconductors have drawn considerations of PV examination bunches worldwide because of its simple and modest creation cost.

Different sorts of sun based cell's energy change productivity from 1976 through 2012 have been reported by National Renewable Vitality Lab (NREL) in Figure 1.

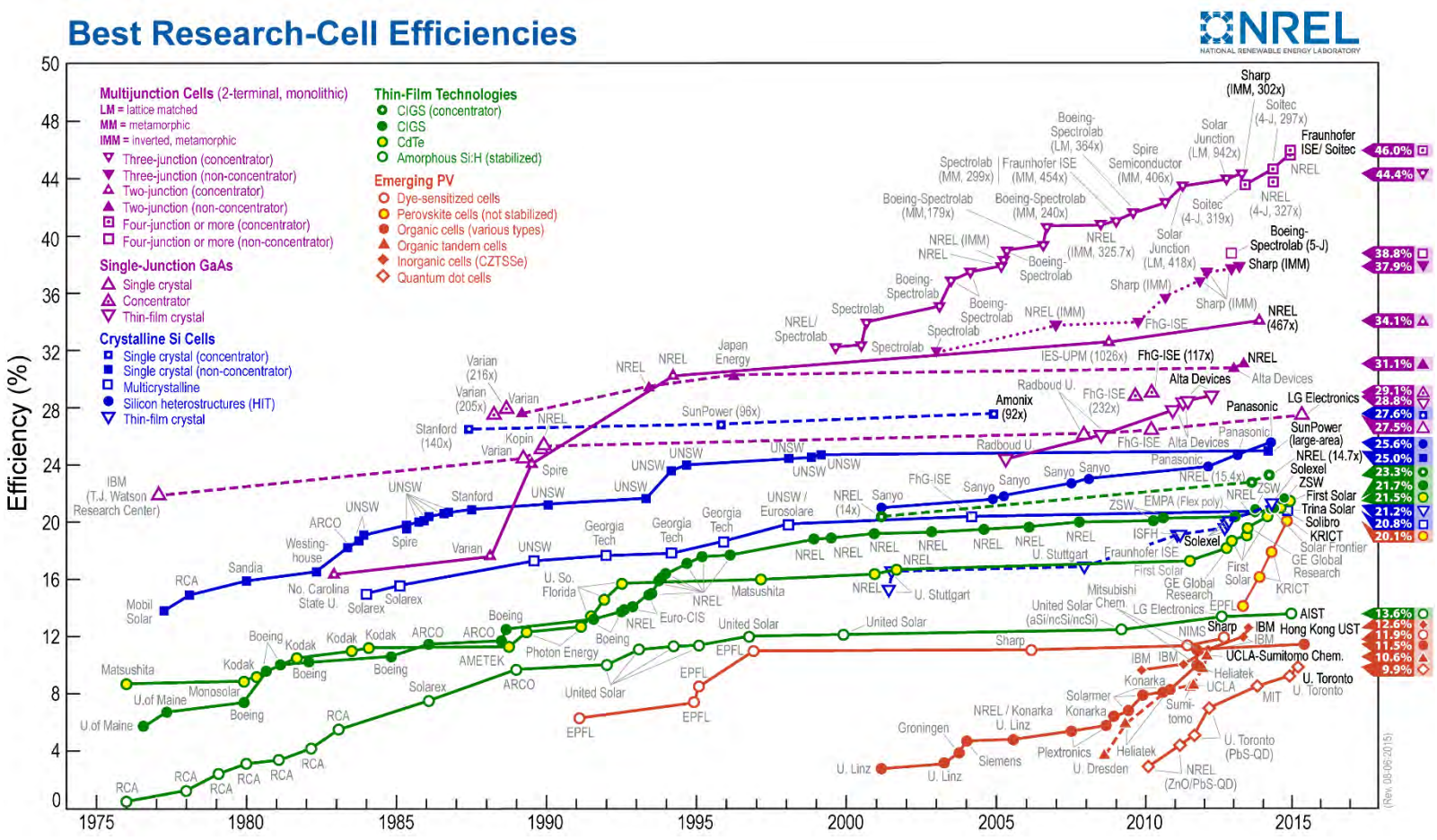

Figure 1: Power Conversion Efficiency for various photovoltaic technologies up to year 2012 (Source: NREL)

1.1.4 Photovoltaic Manufacturing: Present and Future

In the USA, normal expense of framework supplied power in 2009 was 9.5¢/kWh and will keep on ascend because of expansion popular. Three unique rates in cost augmentation are appeared in Figure 2 [8]. Photovoltaic generation has developed at a rate of more noteworthy than 40%/year over the previous decade. Be that as it may, the present cost of power created by PV is 2 to 3 times the expense of framework supplied power yet it keeps on diminishing and anticipated to merge, called framework equality, at some point in this decade (prior to 2020) [8], appeared in Figure 2.

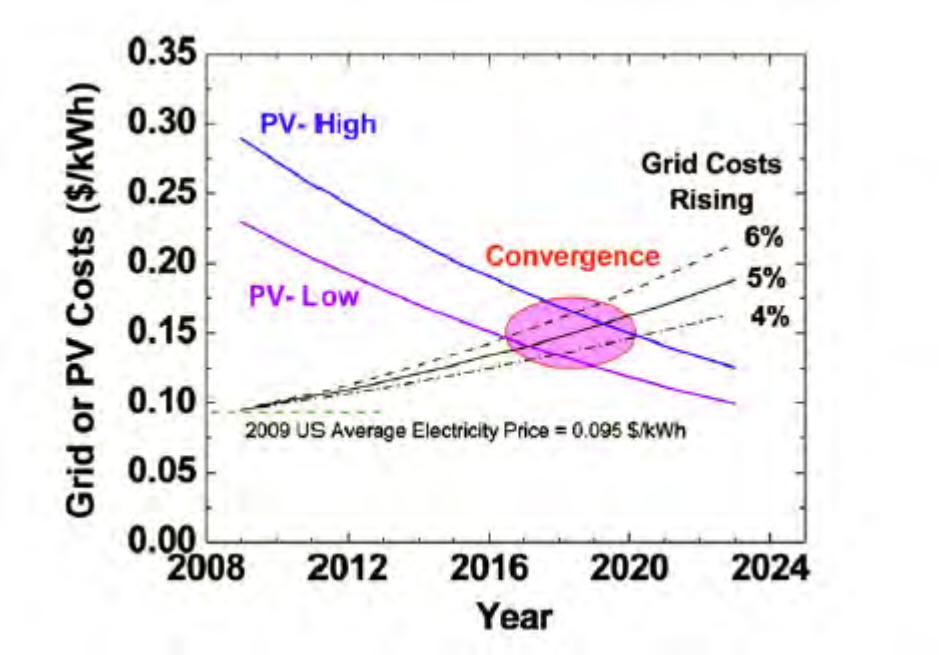

Figure 2: Projected convergence of the cost of electricity produced by PV and the grid prices [8]

1.1.5 Solar Cell Types

Various types of solar cells based on types of materials used are classified briefly in this section.Inorganic bulk semiconductors such as mono- and polycrystalline silicon, amorphous silicon andthin films of semiconductors such as cadmium telluride (CdTe), Copper indium gallium selenide(CIGS) are used as photovoltaic material. Another category of materials include organic dyes andorganic polymers make solar cells of thin film type. The third category uses nanocrystals andused as quantum dots.

1.1.5.1 Solar Cells of Crystalline Silicon

Photovoltaic cells made of silicon are the p-n junction type where electron-hole pair are produced subsequent to retaining photons are driven in inverse bearings by the boundary potential producing a current in the closed circuit. Solar cell based modules produced today for

the most part utilize monocrystalline (c-Si) and polycrystalline silicon (poly-Si) which shared 87% of the PV market in 2011 [9]. Both are discussed below.

• **Monocrystalline Silicon (c-Si):**

Monocrystalline silicon is produced by the Czochralski (CZ) method where a single crystal silicon seed is dipped into a high purity melt of polycrystalline and pulled slowly to form an ingot of single crystal silicon. Single crystal silicon has high lattice uniformity throughout the material resulting in higher mobility of charge carriers. Although, they show a higher power conversion efficiency (up to 25% [10]) compared to poly-Si PV modules, c-Si manufacturing costs are higher. Due to higher thickness requirements and a significant amount of c-Si loss during wafer process, cost of the PV modules becomes even more.

• **Polycrystalline Silicon (poly-Si):**

Polycrystalline silicon has many crystalline grains connected in different orientations. Polycrystalline silicon is made by cooling large molten blocks of silicon. Poly-Si is stronger and can be cut to one-third the thickness of c-Si material making it cost effective. The ribbon growth method directly grows thin sheets of poly-Si that does not require sawing, reducing the cost of the PV module. Irregular grain boundaries in poly-Si hinder the charge mobility causing a decrease in power conversion efficiency. However, its longevity comparable to monocrystalline cousin, lower manufacturing cost and decent conversion efficiency up to 20% [10], such cells are the most popular choice in residential installations.

1.1.5.2 Thin Film Solar Cells

• **Amorphous Silicon (a-Si):**

Amorphous silicon is the most developed of the thin film technologies and its basic electronic structure is p-i-n type. It has a higher bandgap (1.4 - 1.7 eV) and stronger absorption in the visible light because of high absorptivity, even a micron thick amorphous silicon can retain the ma$j_o$rity of the usable daylight, hence diminishes the material expense. Amorphous silicon can

be deposited on low cost substrates such as glass and transparent plastic, and it requires low temperature (≈ 75℃) processes, reducing the production cost drastically. However, disordered a-Si based solar cells suffer from a poor conversion efficiency of about 10% and from significant degradation within few months of sunlight exposure. Amorphous silicon solar cells are about 3% of the world PV market [9].

• **Cadmium Telluride (CdTe):**

It is polycrystalline direct bandgap material made of cadmium (Cd) and Tellurium (Te), which has a band gap of 1.5 eV, a perfect matching material for absorbing sunlight coming to the Earth in terms of optimal conversion to electricity. Since it is difficult to produce thin film of n-type CdTe, a heterojunction of p-CdTe and wide band gap n-type semiconductors are commonly used. The most common heterojunction partner for p-CdTe is wide band gap (2.4eV) n-type CdS thin film. High absorptivity of CdTe film enables sunlight to be fully absorbed by nearly 2μm thick material [8], which reduces the material cost. In addition, relatively easy and cheap fabrication processes such as high-rate evaporation, spray or screen printing are added advantages. An efficiency of more than 17% has been achieved so far [10]. The power conversion efficiency of CdTe based solar modules has disadvantages of its instability and extreme toxicity of cadmium metal during recycling. It represented 6% of the 2011 world market [9].

• **Gallium Arsenide (GaAs):**

It's a compound semiconductor made of gallium (Ga) and arsenide (As) and has a crystal structure same as that of silicon. Due to a high photon absorption coefficient, GaAs requires only a few microns of material to absorb the same amount of light as a 200-300 micron thick crystalline silicon cell. It has high power conversion efficiency too, about 25-30%. A triple junction GaAs cell held the high efficiency record on 15 Oct 2012 [11].

1.1.5.3 Dye Sensitized Solar Cell (DSSC)

The dye sensitized solar cell also known as a Gratzel cell is an electrochemical device. The Gratzel cell was invented by Gratzel at EPFL, Switzerland [12, 13]. A porous bed of titanium dioxide (TiO_2) nanoparticles soaked in a dye solution acts as photoactive layer. Rutheniumpolypyridine is generally used for dye molecules, also called sensitizers. Sensitizers are in contact with a thin layer of iodide electrolyte coated on cathode. When excited by a light photon, the dye molecule injects an electron into the TiO_2 and diffuses towards the external circuit. This loss of the electron is compensated by the iodide electrolyte which regains an electron from the cathode to complete the circuit. DSSC has a very high response in visible light spectrum, so can efficiently work even in diffused light, indoor light or cloudy weather. The liquid electrolyte could be leaky and freeze at low temperatures. A record high efficiency of 12.3% has been achieved [14].

1.1.5.4 Quantum Dot Solar Cell (QDSC)

The electron energies in quantum dots (QDs), which are nanometer sized semiconductor particles, are limited as per quantum mechanics considerations. These energy levels are the bandgaps which can be tuned by changing the size of the QDs without changing the material. The tuning requires simple processes such as varying growth time or temperature. This facilitates QDs to use in multi-junction solar cells to absorb a wider spectrum of photons. Colloidal quantum dots can be synthesized using inexpensive wet chemistry processes. The QD solar cell has a record efficiency of 7% [15].

1.1.5.5 Organic Solar Cell (OSC)

In organic photovoltaic cell (OSCs) [16-23], the active materials are donor (p-type semiconductor) and acceptor (n-type semiconductor) layers. Excitons (excited electron-hole bound pairs) are generated upon absorption of photons and are dissociated at the donor-acceptor (D-A) interface. These separated charge carrier’s transport towards the respective electrodes is

governed by diffusion and the internal electric field. In a single layer OPV device, excitons are dissociated at the metal-semiconductor Schottky barrier whereas in bilayer devices they are dissociated at the donor-acceptor planar junction. A method of improving dissociation of excitons was later developed by making the active layer of intimately mixed active D-A materials together that forms a much larger interface area. Phase segregation is also important for bicontinuous path for charge carriers to reach to electrodes. Organic semiconductors or polymers are inexpensive as they can easily be synthesized in any chemical laboratory. These materials have very high absorption coefficients. Only a few hundred nanometers of material is required to absorb the sunlight efficiently and therefore less material is needed which lowers the fabrication cost further and also enables fabrication of flexible devices. Low efficiency is the one of the major drawback of such cells, yet inexpensive fabrication makes OPV research attractive. A recent rapid growth in overall efficiency has been observed. Heliatek has recently achieved the highest efficiency of 12% by improving its previous record of 10.7% efficiency [24].

2. Organic Solar Cell – General

2.1 Introduction

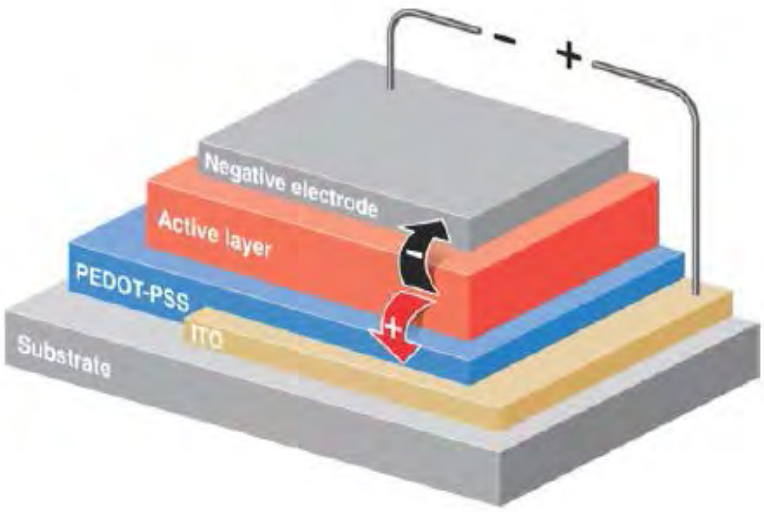

Figure 3: Schematic of an organic photovoltaic cell (source: http://spie.org/x14269.xml)

Figure 3 is a schematic of a typical organic solar cell consisting of a transparent and conductive electrode (usually an ITO anode) with a transparent substrate, an electron blocking layer (such as PEDOT: PSS), an active organic polymer layer (monolayer, bilayer or bulk heterojunction) and a cathode (typically Al or Ca/Al). Light enters through the transparent substrate and charge carriers are generated in the active layer after light absorption and flow towards the respective electrodes. Details of operation are presented in the following sections.

This chapter will describe device operation from light absorption to transport of charge carriers. Various photovoltaic structural designs such as monolayer (or homojunction), bilayer (or planar heterojunction) and bulk heterojuntion will be described. A band energy model under forward and reverse bias, open-circuit and short-circuit conditions will also be explained. The origin of conjugation and semiconductivity in organic materials will be discussed. Atomic and molecular

phenomenon such as excitons and polarons within organic materials will be described. A circuit model with the necessary electrical parameters representing the cell will also be presented

2.2 Principle of Operation

Schematically, Figure 4 indicates loss mechanisms and device operational mechanisms of organic solar cells at various stages from light absorption to charge collection. In the following, we will discuss the five operational steps of organic photovoltaic device, shown in Figure 5.

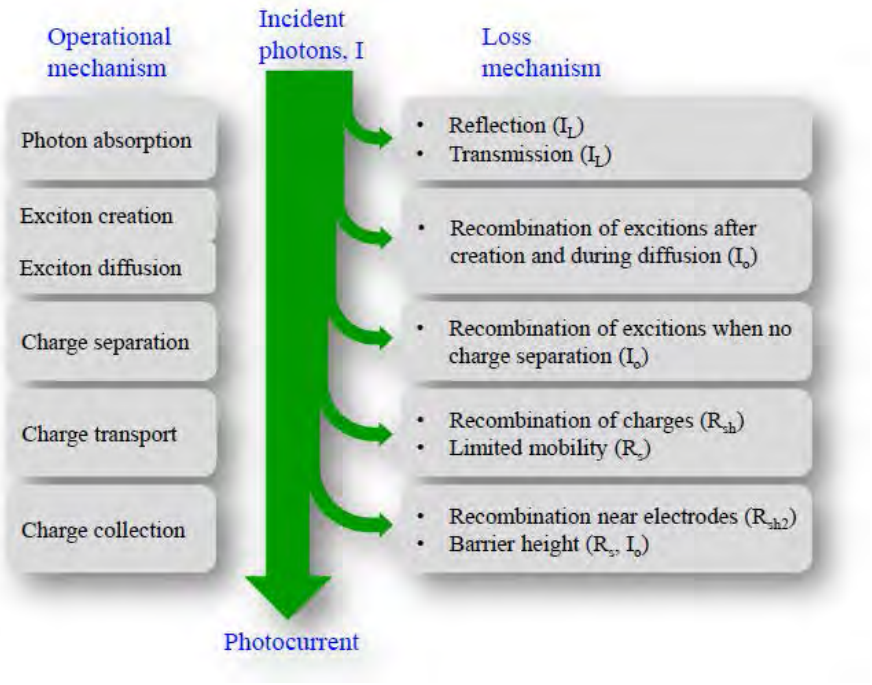

Figure 4: Operational steps and loss mechanism in organic solar cell

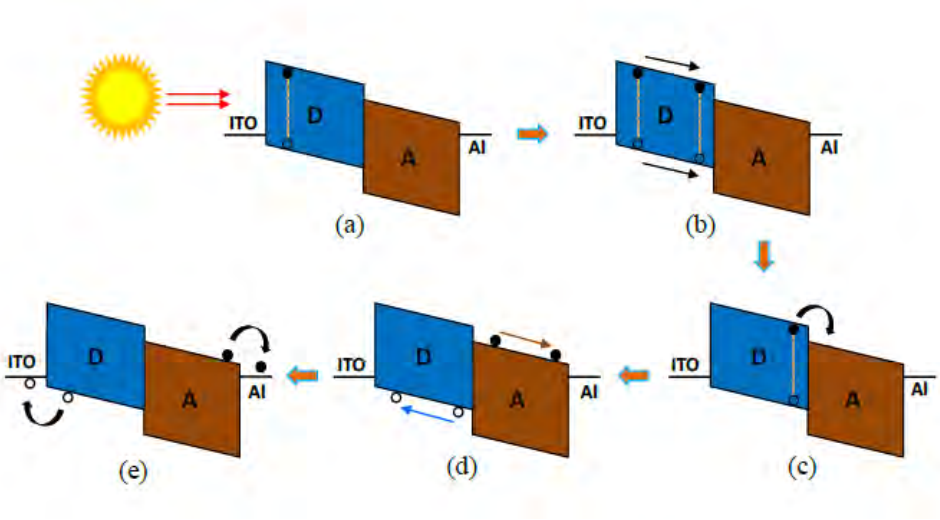

Figure 5: Operational steps of bilayer and bulk-heterojunction OPV cell: (a) Photon absorption and exciton generation (b) Exciton diffusion (c) Exciton dissociation, polaron formation & dissociation (d) Charge transfer (e) Charge collection. Blocking layers are not shown for simplicity.

(a)Photon absorption:

The first step for power conversion from the light is absorption of photons in active layer of the organic solar cell. Incoming photons undergo reflection, absorption and transmission.

(b)Exciton generation and diffusion:

Photon having energy more than or equal to optical band gap of the organic polymer when absorbed, an electron is excited leaving a hole behind but are still attracted strongly by a Coulombic force. This quasineutral particle in a bound state is called an exciton.

The properties of excitons are discussed in Section 2.5. Excitons start diffusing towards a systematically designed interface with another organic polymer or electrode. The excitons diffuse to the donor-accept interface in case of a bulk heterojunction or bilayer device or a

Schottky barrier in the case of a single active layer. The diffusion length must be at least equal to the polymer thickness for excitons to be efficiently dissociated before they are quenched.

(c)Exciton dissociation:

Once excitons reach the interface, they get dissociated due to the local electric field created by difference of electron affinities (EAs) and ionization potentials (IPs) between donor and acceptor material. At the interface, the polymer semiconductor material with higher electron affinity (lower ionization potential) can take electron (hole) from the material having lower EA (higher IP). In other words, after dissociation of an exciton at D/A interface, the electron (hole) from the LUMO (HOMO) of donor (acceptor) transfers to the LUMO (HOMO) of acceptor (donor). Excitons do not contribute to photocurrent if the difference in ionization energies or electron affinities is not sufficient to dissociate them.

(d)Charge transport:

The dissociated charge carriers start moving towards the respective electrodes by diffusion and drift processes. The mobility plays an important role, and is discussed later in this Chapter. At the interface of the organic semiconductor and metal electrodes, the separated charge carriers are collected resulting in a photocurrent.

(e) Charge collection:

The efficiency of charge collection is mostly dependent on the energy band alignment of the donor-HOMO with the anode and the acceptor-LUMO with the cathode. The nature of the semiconductor/electrode interface is complex as interfacial charge density due to dipole formation or chemical reaction at the interface, widely affect the alignment which may or may not favor the charge collection. Efficient charge collection is achieved by using intermediate

layers such as electron and/or hole transport layers that favor unidirectional flow of carriers; and passivation layers to inhibit chemical reaction.

2.3 Device Physics

Below are the diagrams, Figure 6(a) and Figure 6(b) for a general schematic of bilayer and bulk heterojunction OPV devices showing electrodes and various layers used. In bilayer structure, it is always guaranteed that donor and acceptor phase are in contacts with hole and electron transport layer, respectively whereas in bulk heterojunction case, it happens only if bi-continuous or percolated paths exist which is necessary for the cell to work. The bilayer and bulk heterojunction both can be represented by a single energy band diagram, Figure 6(c) as they both differ only in spatial orientation of layers and not energetically. The step by step process of operation is shown via energy band diagram (Figure 6(c)). This section mainly explains about functions of various layers used in the cell. The basic comparison of three different types of OPV structures are explained in next section.

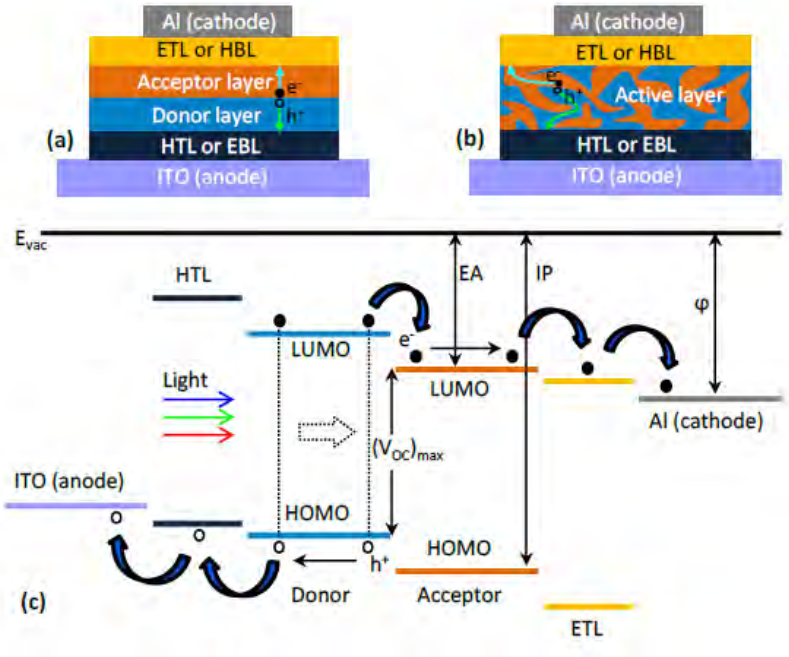

Figure 6: A general schematic of (a) a bilayer OPV cell (b) a bulk heterojunction OPV cell and (c) Energy band diagram of the device

2.3.1 Active Layers for Light Absorption

Active layers are the main constituents of OPV cell which are small molecules or polymer semiconductors. These are also called photo-active layers (or donors and acceptors, explained next) as they can absorb photons with energy greater or equal to optical band gap of the material and generate excitons that are eventually converted to charge carriers. The light absorption can be explained by Beer-Lambert's law which relates the absorption of light through a material having absorption coefficient $\alpha(\lambda)$. If the material is a solid thin film of thickness (d), then $\alpha(\lambda)d > 1$, transmitted light intensity $I(d)$ can be represented by

$$I(d)=I_o e^{-\alpha(\lambda)d} \quad \ldots\ldots\ldots\ldots\ldots\ldots\ldots\ldots\ldots\ldots\ldots\ldots (1)$$

Where, $I_o$is incoming light intensity, $\alpha(\lambda)$ is the wavelength dependent light absorption coefficient and d is the film thickness.

For most efficient absorption of sunlight at earth, the ideal band gap is around 1.4 eV. Most organic semiconducting polymers have band gaps higher than 2 eV (600 nm) which limits the possible absorption to about 30% of the solar spectrum. Organic polymers display orders of magnitude lower mobility compared to inorganic semiconductor crystals and therefore the material has to be very thin in order for excitons to reach the interface without being quenched. Fortunately, a high absorption coefficient (usually > 105 cm^{-1}) of the material partially balances the negative impact of lower mobility in photovoltaic device. Some light trapping methods are also employed to enhance the light absorption [29].

2.3.2 Donor/Acceptor Interface:

At heterojunction, the material with higher electron affinity can take electrons to its LUMO is called acceptor (A). Similarly, the material with lower ionization potential can easily donate an electron from its HOMO, or in other words can take a hole is called donor (D). Meaning, the material with lower (higher) LUMO and HOMO values is donor (acceptor). An electron in donor is excited to LUMO leaving a hole in its HOMO or a hole in acceptor is excited to HOMO leaving an electron in LUMO thus forming an exciton after absorbing a photon. Unlike

conventional solar cells, absorption of photons is not enough to generate free charge carriers and an interface of donor/acceptor (D/A) material with proper energy level matching is required for exciton to dissociate into free charge carriers. The differences in energy levels LUMOs and HOMOs should be larger than exciton binding energy (~ 0.4 eV) for dissociation to occur. Exciton generated in donor (acceptor) material is dissociated at the interface of the organic semiconductors heterojunction by donating an electron (hole) from its LUMO (HOMO) to the LUMO (HOMO) of the acceptor (donor) material and retaining the hole (electron). Exciton dissociation has been described as two-step process: (a) charge transfer to form polaron, i.e. exciton separated into hole and electron in D and A, respectively, but still bound together; (b) polaron dissociation into separated charge carriers (however, polarons may recombine also). The separated charge carriers are then transported to respective electrodes. Therefore, the donors are hole transporting materials or p-type and the acceptors are electron transporting materials or n-type.

If both LUMO and HOMO level of one of the heterojunction organic semiconductor materials is bigger than the other, exciton split is not possible but rather energy transfer will occur in the form of radiation. This situation is desired for designing light emitting diodes (LEDs).

Poly(3-hexylthiophene-2,5-diyl) or P_3HT, poly[2-methoxy-5-(2-ethylhexyloxy)-1,4-phenylenevinylene] or MEH-PPV, copper phthalocyanine (CuPc) are commonly used donors or p-type material in organic electronics. Fullerene (C_{60}), [6,6]-phenyl C_{61} butyric acid methyl ester (PCBM) are common n-type organic semiconductors or acceptors.

2.3.3 Semiconductor/Electrode Interface:

A seminal work of Mott and Schottky has established the theory of metal-semiconductor contact for charge injection from the doped semiconductor to the metal [30, 31]. However, it is not well known to what extent it applies in organic semiconductors, but it is often used to predict the behavior of such contacts for carrier collection or injection. The barrier can be formed at the interface of ITO (anode) and the donor material or Al (cathode) and the acceptor material. A Schottky barrier is formed when metal work function is smaller (larger) than the work function

which is the difference between vacuum level to Fermi level of p-type (n-type) semiconductor, i.e. $\phi_M<\phi_S(\phi_M>\phi_S)$, otherwise the contact is ohmic. Such barriers act as an obstruction to charge carriers which should kept minimum for better charge collection. Charge carriers can overcome the barrier ϕ_B by thermionic emission and/or field emission (quantum mechanical tunneling). The current through the barrier is often described by

$$J=J_o e^{(qV-\phi B)/nkT} \quad \text{.....(2)}$$

where, $J_o$is a constant for low doping and $n \approx 1$ at high temperatures [32], V is the applied voltage and T is the temperature. When the thermal energy $k_B T$is sufficient to produce charge carriers with potential greater than the barrier height ϕ_B ($=|\phi_M - \phi_S|$), thermionic emission occurs. The Schottky barrier is ohmic also when the barrier ϕ_B is very thin or very low. Ohmic contacts are preferred for efficient charge collection for which electrode work functions should be properly matched at donor-HOMO and acceptor-LUMO levels. A large difference between the anode work function and the D-HOMO or the cathode work function and the A-LUMO will cause the loss of open circuit voltage and working potential.

2.3.4 Interfacial Layers:

By inserting a very thin interfacial layer between the electrode and active layer the overall device performance can be significantly improved, Figure 6. Several interfacial buffer layers have been reviewed by Chen et al. [33]. The main functions are described below:

2.3.4.1 Functions of interfacial materials

(a)Injection barrier reduction by interfacial dipole:

The injection barrier $\phi_h(\phi_e)$ is the difference between the metal work function and HOMO (LUMO) of the semiconductor material. Upon introduction of an interface dipole with the positive (negative) pole towards metal the hole (electron) injection barrier can be reduced, shown in Figure 7. Barrier height reduction increases the injection efficiency of carriers in case of

OLEDs and can enhance the open circuit voltage in OPVs. Similarly, the reverse dipole can increase the injection barrier causing an open circuit voltage loss [34, 35].

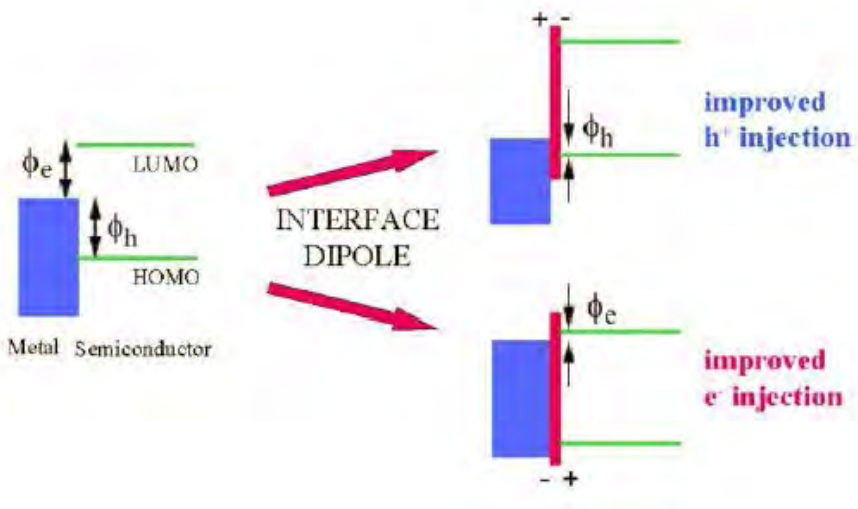

Figure 7: Modification of the hole (electron) injection barrier $\phi_h(\phi_e)$ upon introducing interface dipole (source: [37]).

(b) Blocking layers:

Blocking layers are introduced between the electrode and the active layer of OPV cells to avoid recombination of charge carriers at semiconductor-electrode interface and allow passing certain type of charge carrier, either holes or electrons. An electron blocking layer (EBL), also called a hole transport layer (HTL) is when inserted between the anode and donor layer, only holes could be allowed to reach the anode from the active layer and hence impedes the recombination with electrons at the anode-donor interface. Similarly, insertion of hole blocking layer (HBL) or electron transport layer (ETL) between the active layer and the cathode (Al) can improve the device performance by allowing electron transport only and also hindering exciton quenching at cathode.

(c) Active layer passivation and suppression of diffusion:

Metal ion diffusion into the organic layer has a detrimental effect. The metal/organic interface undergoes chemical reactions that change the contact properties and forms interfacial dipole barriers which can cause kink (S-shape) effects in J-V curves [37]. Therefore a buffer or passivation interlayer is inserted to prevent diffusion and interface reaction.

(d) Modulation of optical field by an optical spacer:

The incident light forms a standing wave inside the active layer of the cell. The transparent optical spacer between polymer and electrode is introduced such that the optical field strength is maximum in active layer zone to enhance the photocurrent [38].

2.3.4.2 Anode interlayers

The most commonly used EBL at anode is poly(3,4-ethylenedioxythiophene): poly(styrenesulfonate) or PEDOT: PSS, a conjugated polymer that is doped by H^+ from PSS has work function of 4.75eV – 5.15eV depending on the doping concentration [39]. PEDOT is conductive (~1000S/cm) and not soluble in water, however, when doped with PSS, it becomes hydrophilic and soluble in water. PEDOT: PSS has a lower conductivity of conductivity ~ 1-10 S/cm. It absorbs little light in the visible region and is widely used as transparent and conductive polymer with ductility. PEDOT: PSS is widely used for coating ITO glasses to smooth their spikiness to avoid shorts in OSCs. The top layer of PEDOT: PSS is PSS- rich phase which is a wide band gap polymer is responsible for blocking the electrons [40] and increased photovoltage [41].

This layer also hinders exciton recombination at the anode resulting in improved photo carrier generation. PCE with optimized thickness of PEDOT: PSS can be 6 times more than the PCE

without it [42]. However, its acidic nature etches the ITO and causes lifetime instability [43, 44]. Its conductivity can be significantly improved by a post-treatment (also called secondary doping) with various compounds, such as dimethyl sulfoxide (DMSO), ethylene glycol (E_g), acids etc. [45, 46]. Molybdenum trioxide (MoO_3) is also used as an EBL due to its low LUMO value (LUMO – HOMO: 2.4eV – 5.3eV) and high transparency and improvement in device performance has been achieved [47-49]. V_2O_3 and MoO_3 as anodic interlayers is are reported as replacements for PEDOT: PSS [50].

2.3.4.3 Cathode interlayers

Aluminum is the most commonly used cathode electrode. Instability of Al was studied by Logdlund et al and Antoniadis et al who found that Al-C bond formation disrupts the π-conjugated system [51, 52]. Formation of a dipole at the interface of Al and PCBM in (P_3HT: PCBM) device increases the extraction barrier and reduces the V_{oc} [34, 35]. A low work function metal, calcium (Ca), makes an ohmic contact when inserted between Al and the polymer, resulting in a higher fill factor [53]. Alkali metal compounds such as lithium fluoride (LiF) and cesium carbonate (Cs_2CO_3) provide low work function contacts [54-56]. A thin layer (~1nm) of LiF acts as dipole modifying the vacuum level to reduce the workfunction of Al which helps in better electron extraction [57] and also serves as a buffer layer to reduce the Al diffusion into the polymer. A more versatile electron injection layer Cs_2CO_3 which can be thermally evaporated or spin coated before cathode layer, be it Al or Ag, shows similar performance [54, 58, 59].

Other commonly used HBLs or ETLs between the polymer and the cathode are bathocuproine (BCP), titanium dioxide (TiO_2), zinc oxide (ZnO). Such materials are able to block holes due to the large HOMO values of BCP (LUMO-HOMO: 3.5 eV – 7 eV), TiO_2 (LUMO – HOMO: 4.4 eV – 8.1eV) or ZnO (LUMO – HOMO: 4.2 eV – 7.5 eV) and inhibit recombination of excitons at the cathode. BCP as an interfacial HBL is also known to be an excellent exciton blocking layer, and can more than double in the PCE [60, 61]. With titanium dioxide (TiO_2) the PCE is enhanced more than twice and also the stability is greatly improved [62, 63]. With ZnO as the HBL an improvement in device performance and stability is reported [47, 64, 65].

2.3.5 Electrode Materials:

The selection of electrode material is crucial and as discussed before, depending on the LUMO/HOMO levels of the Donor and Acceptor materials, the contact could be ohmic or blocking. The difference between anode and D-HOMO or cathode and A-LUMO should be minimized to lower the voltage loss of the cell. Elements in the periodic table with their workfunctions are given in Table 1 [66]. The common cathode electrodes used in organic solar cells are Al, Ca and Mg. Effects of few common cathodes on performance of BHJ solar cell were investigated in [67].

Transparent electrodes are generally hole-collecting anodes and have high work-functions. Indium tin oxide (ITO) is the most widely used transparent conducting anode, which is a degenerate semiconductor comprising a mixture of indium oxide (In_2O_3 – 90%) and tin dioxide (SnO_2 – 10%). It is formed by reactive sputtering of an In-Sn target in an oxygen atmosphere. ITO has a Fermi-level of 4.5 – 4.9 eV and a bandgap of 3.7eV. There is no absorption of light of wavelength longer than 350 nm due to its large bandgap and hence it is quite suitable as a conducting material that is transparent to much of the solar spectrum.

Table 1: Workfunction (eV) of elements in polycrystalline form.

IA	IIA	IIIB	IVB	VB	VIB	VIIB		VIII		IB	IIB	IIIA	IVA	VA	VIA
Li	Be											B	C	N	O
2.9	4.98											4.45	5.0	-	-
Na	Mg											Al	Si	P	S
2.75	3.66											4.28	4.85	-	-
K	Ca	Sc	Ti	V	Cr	Mn	Fe	Co	Ni	Cu	Zn	Ga	Ge	As	Se
2.30	2.87	3.5	4.33	4.3	4.5	4.1	4.5	5.0	5.15	4.65	4.33	4.2	5.0	3.75	5.9
Rb	Sr	Y	Zr	Nb	Mo	Tc	Ru	Rh	Pd	Ag	Cd	In	Sn	Sb	Te
2.16	2.59	3.1	4.05	4.3	4.6	-	4.71	4.98	5.12	4.26	4.22	4.12	4.42	4.55	4.95
Cs	Ba	La	Hf	Ta	W	Re	Os	Ir	Pt	Au	Hg	Ti	Pb	Bi	Po
2.14	2.7	3.5	3.9	4.25	4.55	4.96	4.83	5.27	5.65	5.1	4.49	3.84	4.25	4.22	-
Fr	Ra	Ac	Th	Pa	U										
-	-	-	3.4	-	3.63										
			Ce	Pr	Nd	Pm	Sm	Eu	Gd	Tb	Dy	Ho	Er	Tm	Yb
			2.9	-	3.2	-	2.7	2.5	3.1	3.0	-	-	-	-	-

2.3.5 Operating Steps of OPV Cells

The electrodes are represented by their work functions, and the organic semiconductors by their LUMO-HOMO levels. Four simple device operational steps under different voltage regimes and I-V curve are shown in Figure 8 and Figure 9, respectively.

- **Short circuit condition:**

  When metals shorted together align to same energy level resulting tilting the LUMO-HOMO bands of organic semiconductor layer/layers between electrodes. There is no dark current as no voltage is applied across. The output current is represented by short-circuit current I_{SC}, Figure 9(a). The difference of work functions of the metals creates an internal electric field distributed throughout the device. After excitons dissociation at interface, the holes and electrons are pulled toward higher and lower work function electrode, respectively due to internal field and thus cell generates electricity.

- **Open circuit condition:**

  When dark current or diffusion current counter balances the photocurrent or drift current and output light current is zero. LUMO-HOMO energy bands of the semiconductor are almost flat. The applied voltage in this case is a little below the metal work function difference which opposes the built-in electric field.

- **Reverse bias condition:**

  OPV device extracts more charge carriers under stronger electric field and diode works as a photodetector, i.e. extracted charge carriers or photocurrent is proportional to the light intensity.

- **Forward bias condition:**

  The dark current is almost zero until the open circuit voltage and heavy injection of charge carriers takes place near and after V_{oc}, Figure 9. In this case, there is large recombination and if it is radiative, the device operates as a LED.

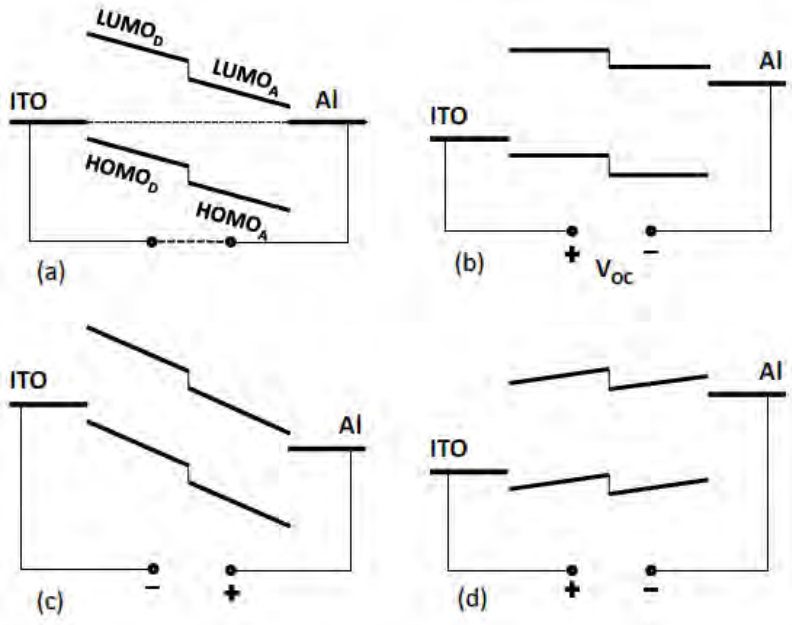

Figure 8: Energy band diagram of a typical OPV cell under (a) short circuit (b) open circuit (c) reverse bias and (d) forward bias.

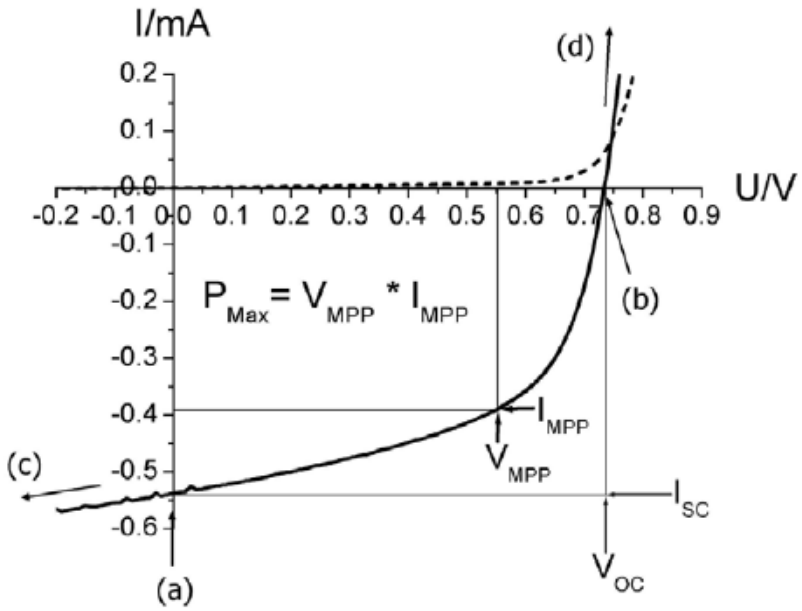

Figure 9: Current-voltage curve of a typical OPV cell (dotted: dark current; solid: illuminated current). (a) short circuit (b) open circuit (c) reverse bias (d) forward bias.

2.4 OPV Architectures:

We will discuss three main types of organic photovoltaic cell structures shown in Figure 10.

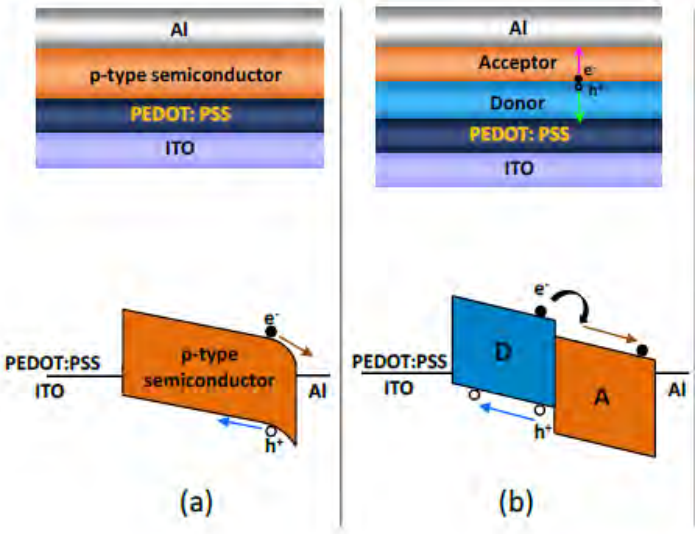

Figure 10: (a) Single layer device (b) Bilayer or planar heterojunction

2.4.1 Single Layer Device:

The first organic solar cells were based on an organic layer sandwiched between two metal electrodes of different work functions. Such type of cells can be explained by the MIM model or by Schottky barrier formation between a metal of low work function and a p-type semiconducting layer. Band bending of organic semiconductor at the semiconductor-metal interface has been confirmed with Kelvin probe study by H. Ishii et al [68]. Figure 10(a) shows a band bending at the interface between the electrode (Al) and the p-type organic semiconductor where electric field is created due to the bend. Excitons which diffuse towards the Schottky barrier can be dissociated into electrons and holes under this field. Schottky-based organic solar cells using phthalocyanine produced very small photocurrents on the order of $20\mu A/cm^2$, under AM1.5 [17, 69, 70]. Single layer type OPV cells suffer from severe exciton recombination due to insufficient electric field to dissociate excitons; and charge carriers recombination as holes and electrons are generated in the bulk which has higher probability to recombine. Organic layer has to be thin enough as excitons generated near the depletion region or in the near range of exciton diffusion length can contribute to photocurrent.

2.4.2 Planar or Bilayer Structure:

In bilayer device, the active layer consists of two organic semiconductors namely the donor and the acceptor stacked together with a planar interface. Such stacking is done by either sequential spin coating of the solution or thermal evaporation of the donor (D) and the acceptor (A). Unlike in the depleted region of p-n junction solar cells, it does not have an in-built electric field at D-A interface due to absence of doping. Excitons in this case are dissociated more efficiently at the donor-acceptor (D-A) interface due to sufficient LUMOs and HOMOs level differences of these two layers, Figure 10(b). Upon photon absorption, excitons are excited from HOMO to LUMO and diffuse towards the D-A junction where an exciton can be separated by donating an electron from the donor to acceptor or a hole from the acceptor to the donor. The dissociation may take place under the condition when the difference of electron affinity (EA) of the acceptor and

ionization potential (IP) of excited state of the donor is greater than exciton binding energy (U_B) or, $(EA)_A - (IP)_{D^*} > U_B$.

Similarly, excitons generated in the acceptor can be dissociated at the interface when $(IP)_D - (EA)_{A^*} > U_B$. An asterisk mark (*) indicates the excited state condition.

Bilayer devices show majority-carrier transport phenomena as after dissociation, the electron is transferred to the acceptor or n-type layer and the hole is retained in the donor or p-type material. Hence, bulk recombination is not possible in this case. A bilayer solar cell made of copper phthalocyanine (CuPc) and fullerene (C_{60}) as a donor-acceptor pair has showed a power conversion efficiency about 3.6% under AM1.5 [71, 72]. Pentacene based bilayer cells showed efficiencies about 1% - 2.7% [25-28].

Due to concentration gradient, excitons once generated diffuse towards the D-A interfaces. The exciton diffusion length is $L_D = \sqrt{(D\tau)}$, where D is diffusion coefficient and τ is the exciton life-time. Very low exciton diffusion length (few tens of nanometers) [73] limits the thickness of the active layers to about hundred nanometer in order to inhibit exciton quenching before reaching the interface of active layers in the bilayer structure.

2.5 Properties of Organic Semiconductors

2.5.1 Properties of Conjugated Materials

(a)Hybridization

The backbone of the molecules of organic materials consists of covalent bonded carbon atoms. The wavefunction of the valence electrons is distorted by the surrounding atoms or molecules and atomic orbitals form new hybrid orbitals. Hybridized orbitals are useful in explaining the shape of molecular orbitals. In methane (CH_4), four electrons (2s and 2p) in the outer shell of the

carbon atom forms four equivalent sp^3 hybrid orbitals and makes four covalent σ-bonds with neighboring hydrogen atoms. The sp^3-orbitals form a tetrahedral structure with an angle approximately 109° between the orbitals. In ethylene ($H_2C=CH_2$), three electrons (1s and 2p) of the C atom form three coplanar and 120° spaced sp^2 hybrid orbitals (Figure 11) to make σ-bonds with four hydrogen atoms. Another two hybrid orbitals form a σ(C-C)-bond when remaining two *p*-orbitals form a π(C-C)-bond, shown in Figure 12(a) and (b).

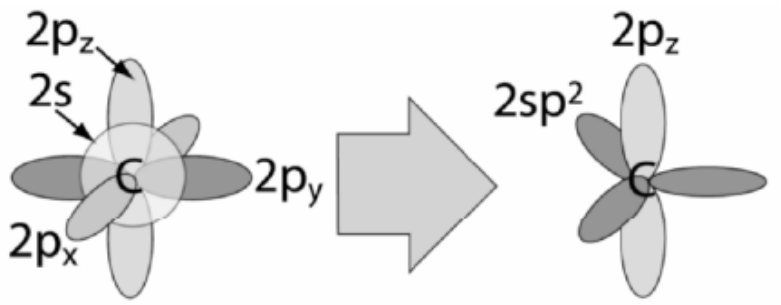

Figure 11: A schematic of sp^2 hybridization of a carbon atom with unhybridized p_z [74].

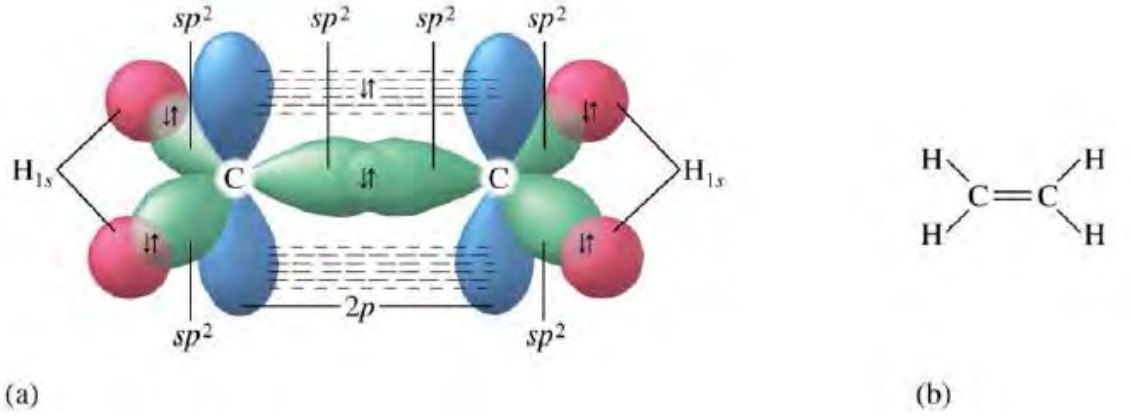

Figure 12: (a) σ and π bonding in ethylene (b) chemical structure

(b)LUMO and HOMO energy levels

When two atoms interact with each other to form a molecule, depending on constructive or destructive interference of the atomic orbitals, new wave functions describing the valence electrons are called molecular orbitals, shown in Figure 13. In case of constructive interference, a finite probability of finding an electron between two nuclei acts as a glue to bind them together. These orbitals are called bonding orbitals. If the atomic orbitals undergo destructive interference, there is no probability to find the electrons between the two atoms, thus positive nuclei repel each other. These orbitals are called anti-bonding orbitals. Energy levels when molecular orbitals are formed, split into two - bonding orbitals which are stabilized and have lower energy levels than original atomic level, and - anti-bonding orbitals which are destabilized that are pushed to higher energy levels. Figure 14 shows few dimerization steps of hydrogen molecules in carbon based compounds where at each step, orbitals are split into bonding and anti-bonding orbitals. For a large chain, orbital energy levels are grouped into two compact orbital bands, called valence band with occupied orbitals and conduction band with unoccupied orbitals. The lowest level of the conduction band is called the Lowest Unoccupied Molecular Orbital (LUMO) and the highest level of the valence band is called the Highest Occupied Molecular Orbital (HOMO). LUMO-HOMO energy level and their difference (band gap) mainly determine the optical and electronic properties of an organic semiconductor.

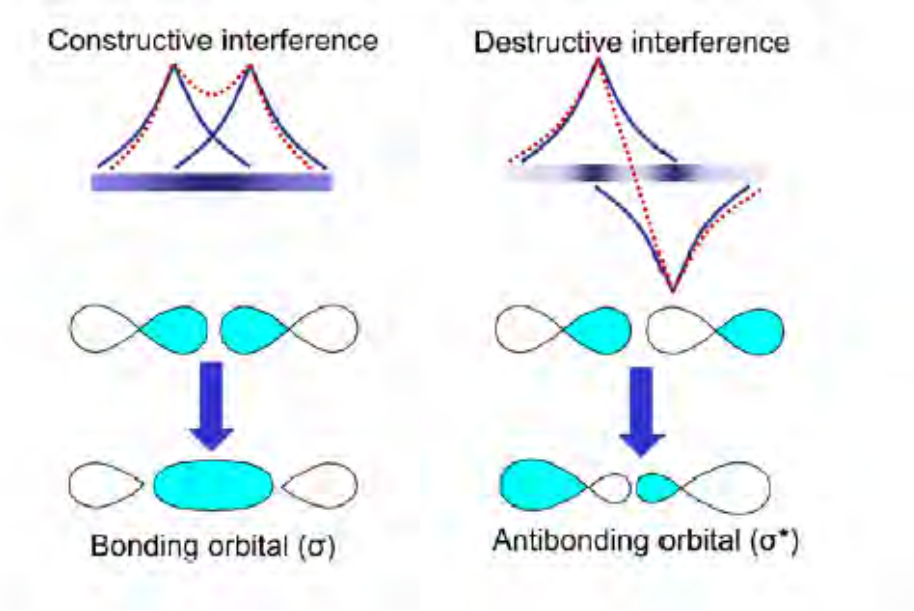

Figure 13: Bonding and anti-bonding orbitals

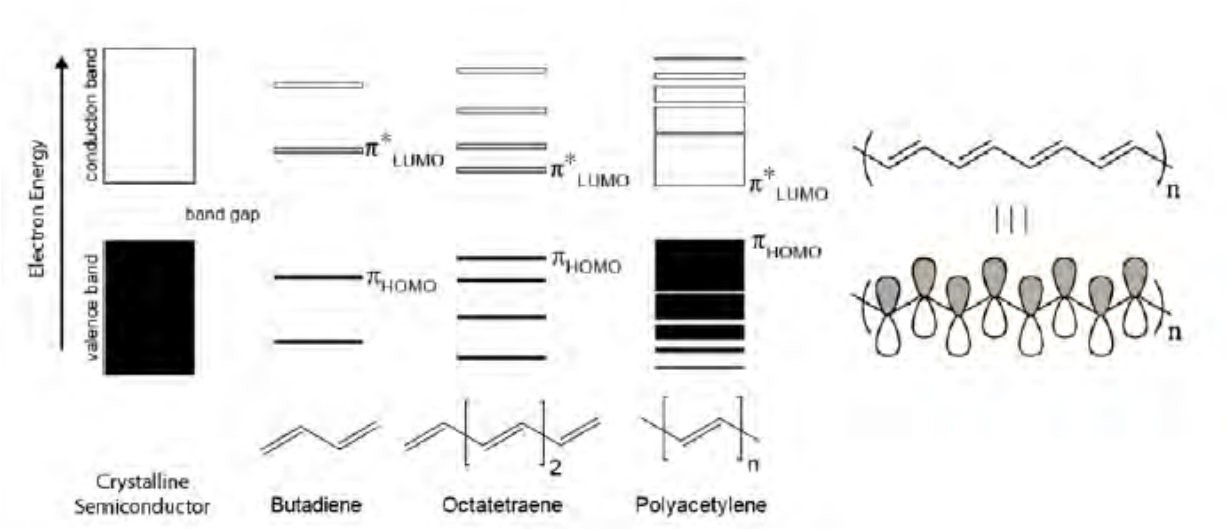

Figure 14: Bonding and anti-bonding energy levels coming together into HOMO and LUMO bands as dimerization length increases. LUMO-HOMO levels are somewhat equivalent to conduction and valence bands in conventional semiconductor (Source: handouts-Excitonic solar cells by Kevin Sivula).

(c) Conjugation

Conjugated molecules have single and double (or multiple) bonds in alternation along their skeleton. Such molecules have connected *p*-orbitals which allow delocalization of π-electrons to lower the overall energy of the molecule and increase stability. The basic structure of a conducting or semiconducting organic material is shown in Figure 15 [74]. The compound may be cyclic, acyclic, or mixed. Butadiene ($H_2C=CH-CH=CH_2$) is one of the smallest conjugated molecules and benzene is (C_6H_6) one of the conjugated cyclic compounds with carbon based skeleton. Conjugated systems can easily donate or except delocalized π-electrons and these polymers are widely used in donor-acceptor based photovoltaic devices. The large conjugated systems include conductive and semiconducting polymers, carbon nanotube, fullerene etc. The larger is the conjugated π-system, smaller is the bandgap, in general.

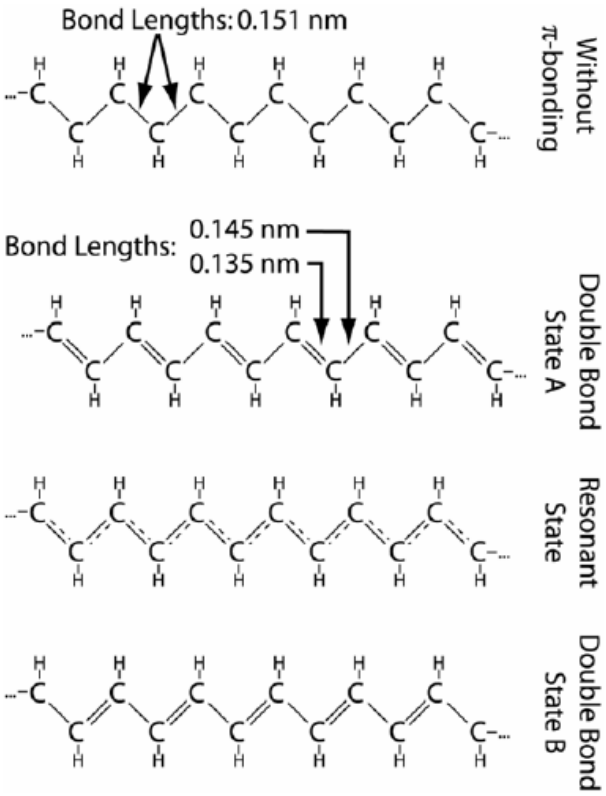

Figure 15: A schematic of the simplest conjugated polymer molecule, transpolyacetylene [74]. The polymer molecules are more stable by interchanging the position of single and double bonds.

2.5.2 Excitons:

Unlike conventional semiconductors where free electron-hole pairs are generated upon light absorption, organic semiconductors create excitons which are essentially quasi-neutral electrostatically bound electron-hole pairs and are not free carriers. The exciton binding energy is about 0.3-0.5eV in organics compared to 0.01eV in conventional semiconductors. To understand more about excitons it is important to examine the difference between conventional semiconductors (CSC) and excitonic semiconductors (XSC).

A charge carrier becomes free when its thermal energy $k_B T$is equal to or greater than the electrostatic potential energy. For a critical distance r_c between charge carriers:

$$E=(q^2/4\pi\varepsilon\varepsilon_o)(1/r_c)=k_bT \quad \ldots\ldots (3)$$

where, q is the electronic charge, ε and $\varepsilon_o$are relative and absolute permittivities, respectively. "In a semiconductor with hydrogen-like wavefunctions, the Bohr radius of the lowest electronic state is" [75]

$$r_B=r_o\varepsilon(m_e/m_{eff}) \quad \ldots\ldots (4)$$

where, r_o (= 0.53 Å) is the Bohr radius of a hydrogen atom in its ground state, m_e and m_{eff} are the free electron mass in vacuum and effective mass in the semiconductor, respectively. For XSC, effective mass m_{eff} is more than me but is opposite in case of CSC. Rearranging the above two equations and we define a ratio γ [75]

$$\gamma=r_c/r_B=[q^2/(4\pi\varepsilon_o r_o m_e k_B)][m_{eff}/(\varepsilon^2 T)] \quad \ldots\ldots (5)$$

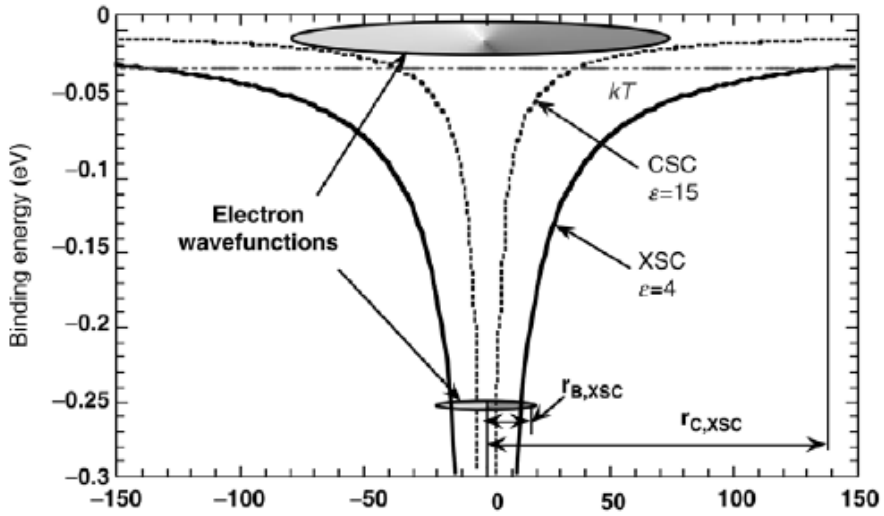

Figure 16: A schematic representing CSCs and XSCs. Wavefunction (r_B) and critical distance (r_c) depend on effective mass, permittivity and the temperature [75]

When $\gamma > 1$, $r_c > r_B$ indicates carriers are not free which is the case for excitonic semiconductor (XSC), and for $\gamma < 1$, $r_c < r_B$ indicates carriers are free suggesting the case in conventional semiconductor (CSC). Although the ratio of r_c/r_B in above equation is only a rough approximation as parameters r_c, r_B, ε, and m_{eff} do not actually have spherical symmetry for XSC, but it's a useful interpretation showing parameters mainly indicate the conditions when excitonic or conventional semiconductors behavior is observed.

According to equations in previous expressions of r_c and r_B, lower relative permittivity ε of XSCs accounts for larger critical distance r_c at a fixed temperature, and the wavefunction r_B is lower for XSC due to its lower value of ε and higher effective mass m_{eff}, indicates $r_c \gg r_B$. Similarly, inverse temperature dependence suggests that at very low temperature T, even CSCs turn into XSCs as $r_c \gg r_B$.

2.5.3 Polarons and Polaron Excitons:

The polarization in a lattice occurs due to electrons repelling its neighboring electrons or negative ions while being attracted towards the nuclei or positive ions in the vicinity. When electron moves through the lattice, it carries the induced polarization as a unit called a polaron, Figure 17. This acts as a potential well which hinders the charge movements and hence decreases the mobility. “In a conjugated molecule, a charge is self-trapped by deformation it induces in the chain. This mechanism of self-trapping is often described through the creation of localized states in the gap between the valence (HOMO) and the conduction (LUMO) bands, as shown in Figure 18 in the case of polythiophene” [76]. A bound pair consisting of an electron polaron and a hole polaron is called a polaron exciton or polaron pair and usually referred to an intermediate state between exciton and dissociated charge carriers.

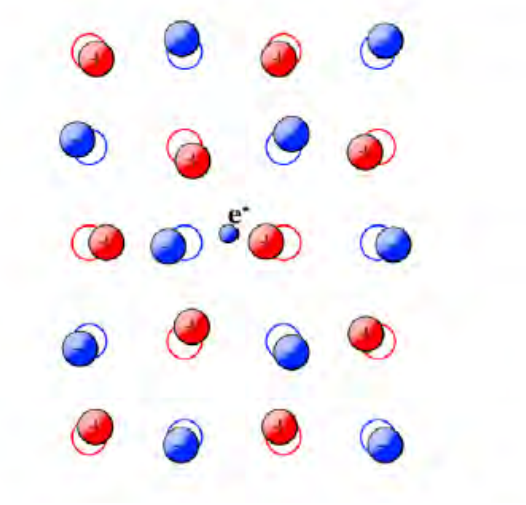

Figure 17: Artist view of a polaron (source: Wikipedia)

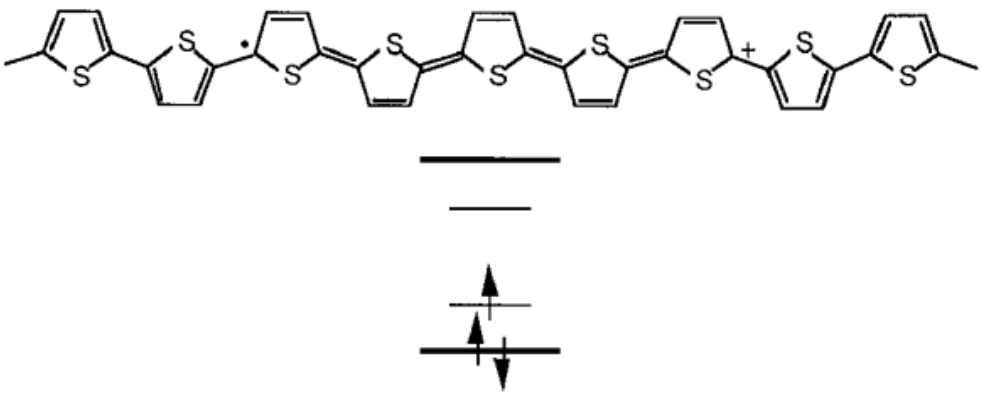

Figure 18: A polaron in polythiophene. *Top*: Change in chemical structure. *Bottom*: Corresponding energy diagram where localized states are created due to polaron formation [76].

2.6 Photovoltaic Cell Parameters

2.6.1 Equivalent Circuit Diagram

Equivalent circuit diagrams (ECDs) are used to characterize the electrical behavior of semiconductor devices with a network of electrical components. A solar cell can be modeled as a diode in parallel with a constant current source and a shunt resistor, and a series resistor shown in Figure 22.

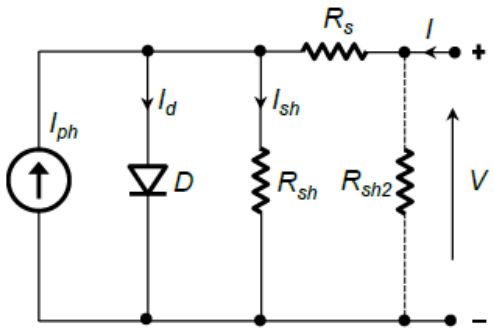

Figure 19: Equivalent circuit diagram for a photovoltaic cell

- **Current source I_{ph} and diode *D*:** I_{ph} = photocurrent generated by the current source upon illumination before any recombination can take place. I_d= current through the diode *D*. $I_{sh}$and I = current through the shunt resistance $R_{sh}$and $R_s$respectively. I and V = output current and voltage, respectively. We can formulate the relation:

$$I + I_{ph} = I_d + I_{sh} = I_d + \frac{V - IR_s}{R_{sh}} \quad \text{..... (6)}$$

where, current through the ideal diode *D* is given by Shockley diode equation:

$$I_d = I_0\left(e^{\frac{q(V-IR_s)}{nkT}} - 1\right) \quad \text{.....(7)}$$

Rearranging the above two equations, we get the expression of output current I with function of output voltage V:

$$I = \frac{R_{sh}}{R_{sh} + R_s}\left[\frac{V}{R_{sh}} - I_{ph} + I_0\left(e^{\frac{q(V-IR_s)}{nkT}} - 1\right)\right] \quad \text{.....(8)}$$

The short circuit current I_{SC} ($I|_{V=0}$) reduces to photocurrent I_{ph} considering diode current is negligible in this case.

- **Shunt resistors R_{sh} and R_{sh2}:** Loss due to recombination of charge carriers near the dissociation sites is represented by R_{sh}. For very small voltages, the diode D does not conduct and the shape of the I-V curve is mainly dominated by the shunt resistance (given $R_{sh} \gg R_s$) which can be derived to:

$$R_{sh} \approx \left[\frac{dI}{dV}\right]^{-1}_{V\approx 0} \quad \ldots\ldots\ldots\ldots\ldots\ldots\ldots\ldots \text{(9)}$$

Sometimes an extra shunt resistor R_{sh2} at the output is also considered representing shorts caused by pinholes or conductivity of the bulk material. It also accounts for recombination losses near the electrodes.

- **Series resistor R_s:** Mobility of the charge carriers in PV cell or conductivity can collectively be transferred into a series resistor R_s. It can be adversely affected by space charges, traps, barriers at contacts or thickness of the transport layers. The slope of the I-V curve can be expressed as:

$$\frac{dI}{dV} = \frac{R_{sh}}{R_{sh} + R_s} I_d \frac{q}{nkT}\left(1 - R_s \frac{dI}{dV}\right) \quad \ldots\ldots\ldots\ldots\ldots\ldots\ldots\ldots\ldots\ldots \text{(10)}$$

For high forward bias voltages, diode current $I_d \gg I_{sh}$ and the shape of the I-V curve is dominated by series resistor R_s and the above equation can reduced to:

$$R_s \approx \left[\frac{dI}{dV}\right]^{-1}_{V \geq V_{OC}} \quad \ldots\ldots\ldots\ldots\ldots\ldots\ldots\ldots\ldots\ldots\ldots\ldots\ldots\ldots\ldots\ldots \text{(11)}$$

To achieve high fill factor, low series resistance and high shunt resistance is desirable.

2.6.2 Open Circuit Voltage:

The open circuit voltage is mainly governed by two energy levels: (1) the effective band gap which is the difference of LUMO level of acceptor and HOMO level of donor ($E_{g,DA}$= $LUMO_A$ –$HOMO_D$), and (2) the difference of the work functions of the electrodes (ΔW_f). In case of bulk heterojunction (BHJ) the bands are parallel which is true for very fine intermixing of the blend constituents. In contrast, a band bending is possible for bilayer solar cells as D-A has only one heterojunction interface and there is large layer width for space charge formation [77].

Cheyns et al considered the thermionic emission at the injection barriers and showed that band bending effect is nullified by injection barriers [78]:

$$V_{OC} = \frac{E_g}{q} - \frac{kT}{q} \ln\left(\frac{N_A N_D}{n_i p_i}\right) \quad \text{……………………………………………. (12)}$$

Here, $E_g$is the effective bandgap; kT/q is the thermal voltage; $N_D$and $N_A$are the effective density of states (DOS) of donor and acceptor, respectively, $p_i$and $n_i$are the hole and electron concentration respectively at the D-A interface.

For BHJ, Koster et al derived the equation for V_{oc} which is based on the quasi-Fermi level difference [79]:

$$V_{OC} = \frac{E_g}{q} - \frac{kT}{q} \ln\left(\frac{(1-P)\gamma N^2}{PG}\right) \quad \text{…………………………………………. (13)}$$

Here, P is the exciton dissociation probability; G is the exciton generation rate; N is the effective density of states; γ is the Langevin recombination strength.

Scharber et al. determined V_{oc} = $|HOMO_D - LUMO_A|/q$ – 0.3 V[80]. The difference of 0.3eV below the effective band gap includes the energy needed for exciton dissociation, energetic disorder and band bending due to charge carrier diffusion.

2.6.3 Efficiencies and Fill Factor:

The sum of the total absorptance (A), transmittance (T), and reflectance (R) must be unity, $A + T + R = 1$. Absorptance of the active layer, η_A= number of photons absorbed in the layer/number of incident photons to the cell.

Internal Quantum Efficiency (IQE) is the quantity defined by ratio of number of electrons in external circuit to number of photons absorbed.

External quantum efficiency EQE or Incident Photon to Current Efficiency (IPCE) of the device is defined by the ratio of number of electrons generated to incident photons in a given time. EQE includes optical losses such as transmission and reflection. This is experimentally determined and measured for monochromatic light. Number of electrons generated/cm^2.s = J_{sc}/e, where J_{sc} is short-circuit current density (A/cm^2) and e is an electronic charge (C). Number of photons generated/cm^2.s = I_λ/E_λ, where, I_λ is the incident light intensity (W/cm^2) and E_λ (=1240×e/λ) is the energy (J) of a photon of wavelength λ (nm), respectively. Therefore,

$$IPCE = 1240.J_{SC}/(\lambda.I_\lambda)$$
$$EQE = \eta_A.IQE$$

…….. (14)

Quantum efficiencies relate the electrical sensitivity of the solar cell to particular wavelength of light and they are often measured over a range of wavelengths. QE does not give information of the overall power conversion efficiency with respect to incident light power.

Power conversion efficiency (PCE) which is the most important parameter in photovoltaics is defined by the ratio of the maximum attainable electric output power from the cell to incident power of light spectrum of interest (or sunlight) to the cell. The current density versus output voltage; and output power versus output voltage has been shown in Figure 23. At point (V_m, I_m) the output power $P_m = (I_m \times V_m)$ is maximum. For a PV cell, the quality of shape of I-V curve is defined by the ratio of the maximum power that can be drawn from the cell and the maximum

ideal power output ($I_{SC} \times V_{oc}$). This ratio is called the cell's fill-factor, $FF = (I_m \times V_m)/(I_{SC} \times V_{oc})$. The power conversion efficiency (PCE) for input power P_{in} is defined:

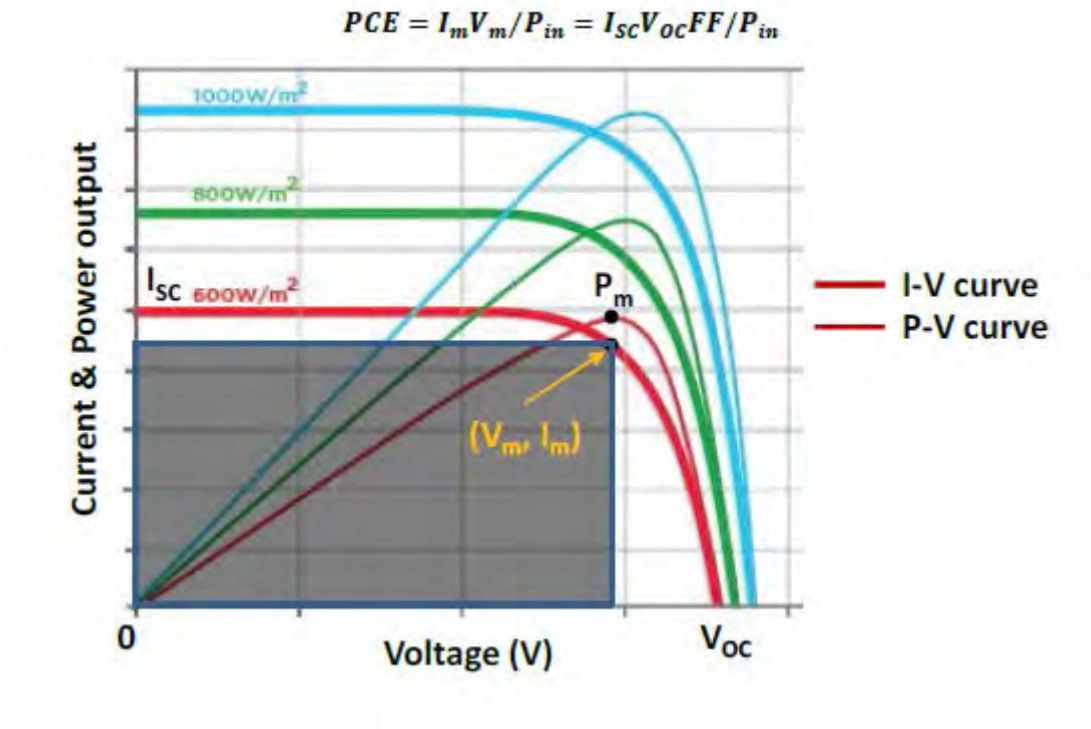

Figure 20: Current and output power versus terminal voltage, i.e. I-V and P-V curve.

If bandgap is wider, open circuit voltage is more. But photons with energy smaller than the bandgap will not be absorbed therefore photon absorption will be less that will lead to reduced short circuit current and vice versa. There must be an optimal bandgap for a given illumination spectrum for which efficiency is at maximum. Shockley and Queisser were the first who theoretically calculated the maximum PCE of 33.7% for a semiconductor with a bandgap of 1.34eV and 29% for silicon with bandgap of 1.12eV [81].

3. Device Model for Organic Solar Cell

3.1. Introduction

The structure consists of bilayer morphology, or a Planar Heterojunction (PHJ) [82], conformed by two organic semiconductors between two electrodes with different work function. One of the organic semiconductors acts as a donor layer (D) and the other as acceptor. Typically the organic materials used in this kind of solar cells are P_3HT (for the donor) and PCBM (for the acceptor)[83].

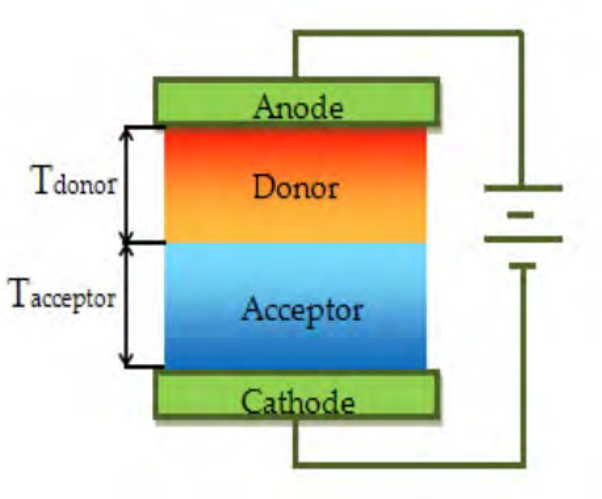

Figure 21: Bilayer Organic Solar Cell (Planar HeteroJunction)

To calculate the I-V characteristics of the OPV cell the following procedure [84]:

1) Optical absorption inside the device is calculated by the transfer matrix method. The absorption profile depends on the complex refractive indices and the thicknesses of various layers in the cell.

2) Exciton diffusion equation is then solved in both donor and acceptor layers. Exciton concentration at the donor-acceptor interface is set to zero with the assumption that exciton dissociation probability is unity and field independent.
3) Charged carrier transport is simulated by the self-consistent solution of drift-diffusion and Poisson equation. Generation term in the carrier continuity equation is calculated from the exciton flux at the DA interface and the recombination of free carriers at the D-A interface is implemented by bi-molecular recombination. We ignore geminate recombination at the interface.
4) The operating temperature is fixed at T_{op} = 300 K. The input irradiance is assumed 1 kW/m^2 for efficiency calculation.

3.2. Basic operation and device Physics:

OPV operation can be divided in four steps: Photon Absorption, Exciton Diffusion, Charge Separation and Carrier Transport. These steps are shown in Figure 22.

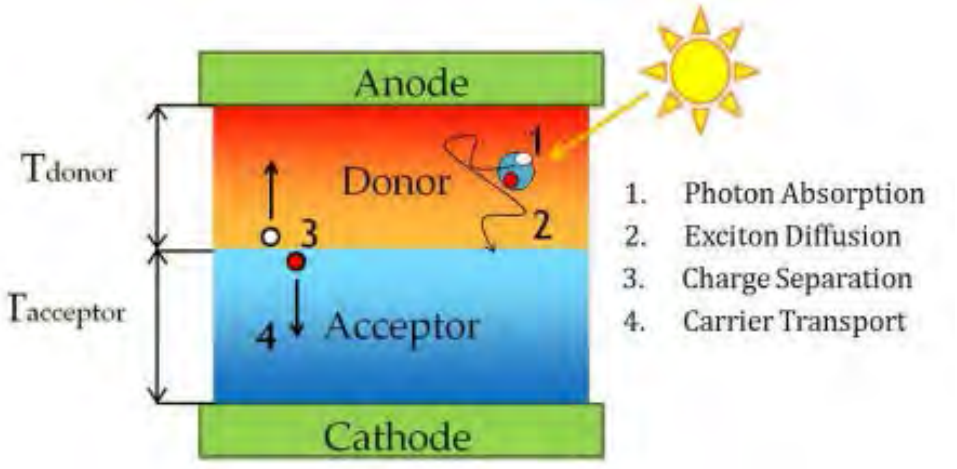

Figure 22. Operation of a bilayer Organic Solar Celll

Following each one of these steps is described:

- **Photon Absorption**

  Photon absorption process occurs when the incident light is absorbed within the photoactive layer of an organic solar cell. In the tool we assume AM1.5 solar radiation as the incident spectrum. We then use transfer matrix method [85] to calculate the absorption in different layers of the cell. The absorption profile depends on the complex refractive indices and the thickness of the various layers in the cell.

- **Exciton diffusion**

  Photon absorption creates a tightly bound electron hole pair called exciton in the organic semiconductor. As the exciton is charge neutral, it moves by diffusion in the active layer. In the tool, exciton diffusion is modeled by the following equation:

$$D_{ex}\nabla^2 n_{ex} = G_{ex}(r) - R_{ex}(n_{ex}) \quad \ldots\ldots\ldots\ldots\ldots\ldots\ldots (15)$$

Where,

G_{ex} : Exciton generation

$R_{ex} = n_{ex}/\tau_{ex}$: Exciton recombination

n_{ex}: Exciton concentration

τ_{ex}: Exciton life time

D_{ex}: Exciton diffusion coefficient

The exciton diffusion length, which indicates the distance the exciton can travel without recombining or decaying, can be defined as:

$$L_{ex} = \sqrt{D_{ex}\,\tau_{ex}} \quad \ldots\ldots\ldots\ldots\ldots\ldots\ldots \quad (16)$$

In organic materials, the diffusion lengths are limited to 5-20 nm approximately [85].

- **Charge Separation**

  Photo-generated excitons are dissociated into electrons and holes at the donor-acceptor heterojunction. We assume the exciton dissociation probability at the heterojunction is high enough that exciton concentration at the donor-acceptor interface is zero. Thus, only the excitons generated within a distance of exciton diffusion length from the heterojunction can contribute to the photo current generation.

- **Carrier Transport**

  Once the exciton has been dissociated, the holes travel though the donor, and the electrons trough the acceptor. Carrier transport is driven by the electric field across the active layer, which is originated by the work function difference between the two electrodes. Carrier transport is modeled by the following equations:

  Drift-Diffusion Transport Equations:

$$J_e = e\mu_e n(x)E(x) + eD_e\nabla n(x) \quad \ldots\ldots\ldots\ldots\ldots\ldots\ldots \quad (17)$$

$$J_h = e\mu_p p(x)E(x) - eD_p\nabla p(x) \quad \ldots\ldots\ldots\ldots\ldots\ldots\ldots \quad (18)$$

Electric field, E(x) is calculated by solving Poisson equation self-consistently with the transport equations. In the above equations:

μ_p :Hole Mobility

μ_e : Electron Mobility

D_p: Hole diffusion coefficient

D_e: Electron diffusion coefficient

n (x): Electron concentration

p (x): Hole concentration

E (x): Electric field

Boundary conditions:

$$n(d) = n_{Al} = N_c \exp\left(-\frac{\Phi_C - \chi_{acceptor}}{kT}\right) \quad \text{..... (19)}$$

$$p(0) = p_{ITO} = N_V \exp\left(-\frac{\Phi_A - \chi_{donor}}{kT}\right) \quad \text{.....(20)}$$

4 ResultAnalysis:

4.1 Discussion on the effective Hole mobility of P_3HT:CNT composite:

Figure 23 shows the effect of adding CNT to a P3HTcomposite. The highest effective hole mobility of a P3HT:CNTcomposite was seen at 1wt% SWCNT concentration. The effective hole mobility of the P3HTcomposite is seen to decrease for higher concentrations of SWCNT.

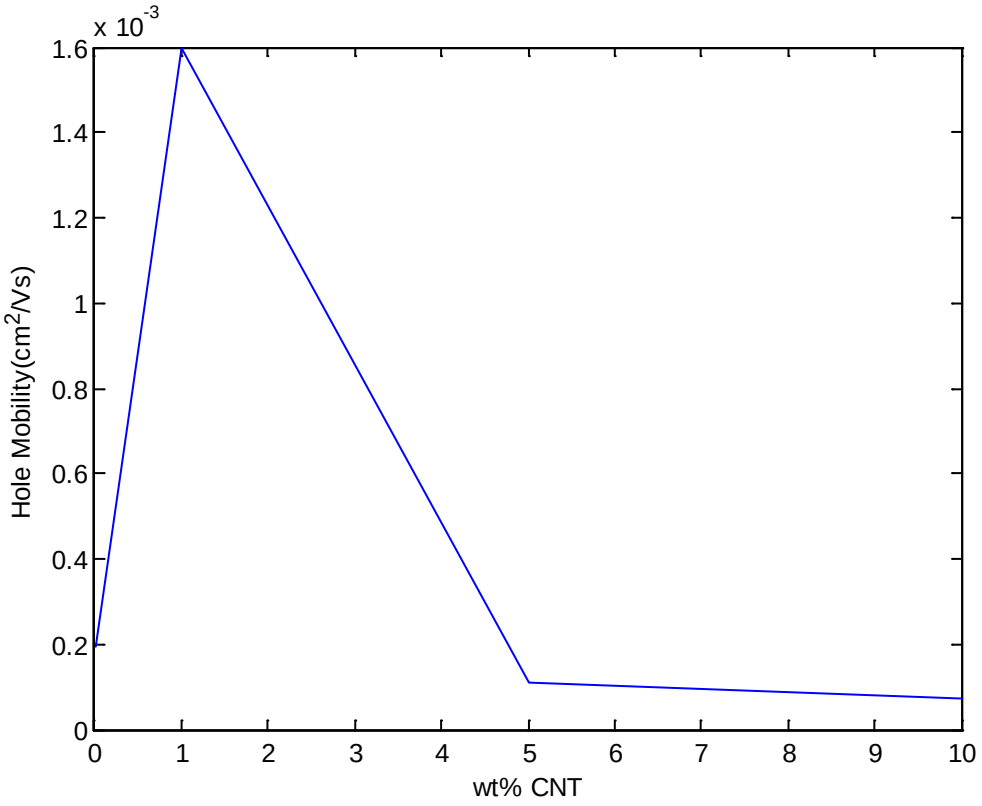

Figure 23: Change in effective hole mobility with increasing weight percentage of CNT

4.1.1 Increased hole mobility and dissociation probability at 1 weight percentage CNT:

The improvement in the effective hole mobility of the P_3HT:CNT composite for CNTs concentration less than 1wt% can be attributed to CNTs 1) ballistic properties which leads to the formation of percolating pathways in the P_3HTmatrix. The presence of percolating pathways via nanotube leads to greater electrical conductivity leading to an efficient charge extraction out of the device through the cathode and 2) No ground state charge transfer takes place between CNT and P3HTindicating that CNTs can form type-II heterojunction with P3HT.The formation of the type II heterojunctions leads to an increase in dissociation probability in the active layer composite.

4.1.2 Decreased hole mobility and dissociation probability for CNT concentration greater than 1weight percentage:

Despite CNTs capability to form type II junction and percolating pathways in the P3HT matrix, the effective hole mobility and dissociation probability of P3HT:CNT composite with concentrations of CNT higher that 1wt% can be seen to decrease. The drastic decrease in the effective hole mobility and dissociation probability is primarily due to the following reasons:

- **Presence of metallic SWCNTs in the P_3HT: CNT composite. [1]**

Unlike s-SWCNTS there exists a considerable ground state charge transfer between P3HT and m-SWCNTS. This particular characteristic of m-SWCNT leads to the formation of EHP trap sites in the band gap of the P3HT:PCBM composite resulting in an increase in EHP recombination and lower effective hole mobility.

- **SWCNTs natural tendency to form aggregates of um scale**

The presence of SWCNT aggregates reduces the amount of interface available for the dissociation of excitons, the degree of aggregation tends to increase with higher content of SWCNTs and hence the exciton dissociation probability decreases with increasing SWCNT concentration. Theoretically in a mixed configuration 2/3 of the total SWCNTs are semiconducting in nature and the rest 1/3 display metallic properties. For the P_3HT:CNT interface to facilitate the exciton dissociation process, the ratio of P3HT:s-SWCNT interfaces should outweigh the ratio of P3HT:m-SWCNT.This requirement is satisfied at 1weight percentage CNT and hence an increase is dissociation probability and hole mobility is noticed in fig 36, but the same principle cannot be applied for P3HTCNT composites with higher SWCNT concentration's (x>1%), reason being that as the concentration of SWCNTs increases in the active layer composite, the majority of interfaces formed will be with m-SWCNTS ,because if multiple s-SWCNTS interact with one another or with m-SWCNTs they become semi-metallic in nature. The presence of m-SWCNTs as mentioned earlier results in the formation recombination centers, leading to a decrease in effective hole mobility and dissociation probability.

4.2 Effect of changing CNT weight percentage on Diffusion Length of Bilayer solar cell

In figure 24 the highest diffusion length is observed at 1wt%. Further increase in wt% decreases the diffusion length. Till 1wt% the mobility increases but further increase in CNTwt% the mobility decreases and since diffusion length is a function of mobility the diffusion length also decreases.

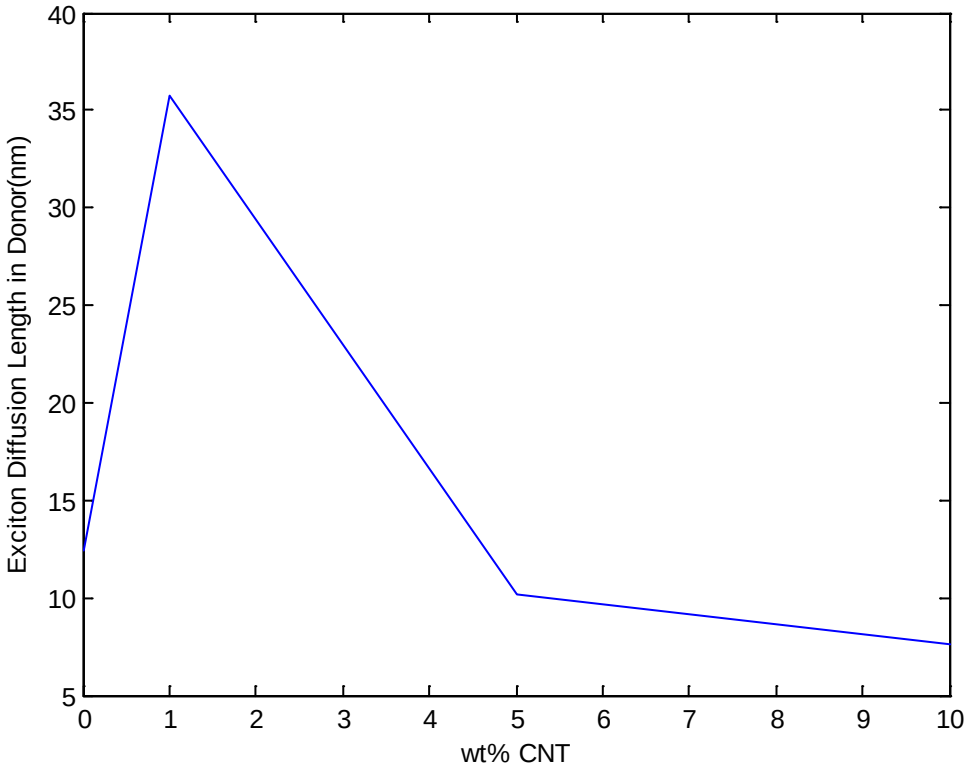

Figure 24: Change in Exciton Diffusion Length with increasing weight percentage of CNT

4.3 Effect of changing CNT weight percentage on Bi-molecular recombination coefficient of Bilayer solar cell

An important loss mechanism in organic solar cells is the non-geminate recombination of free charges. The rate of the bimolecular recombination depends quadratically on the charge density and it is determined by the time required for electrons and holes to diffuse towards each other. In figure 25 we got the maximum peak at 1weight percentage. Further increase in CNT semi metallic proportion increases. As we do not get pure CNT in nature so the problem of aggregation occur which increases the hole pair recombination centre.

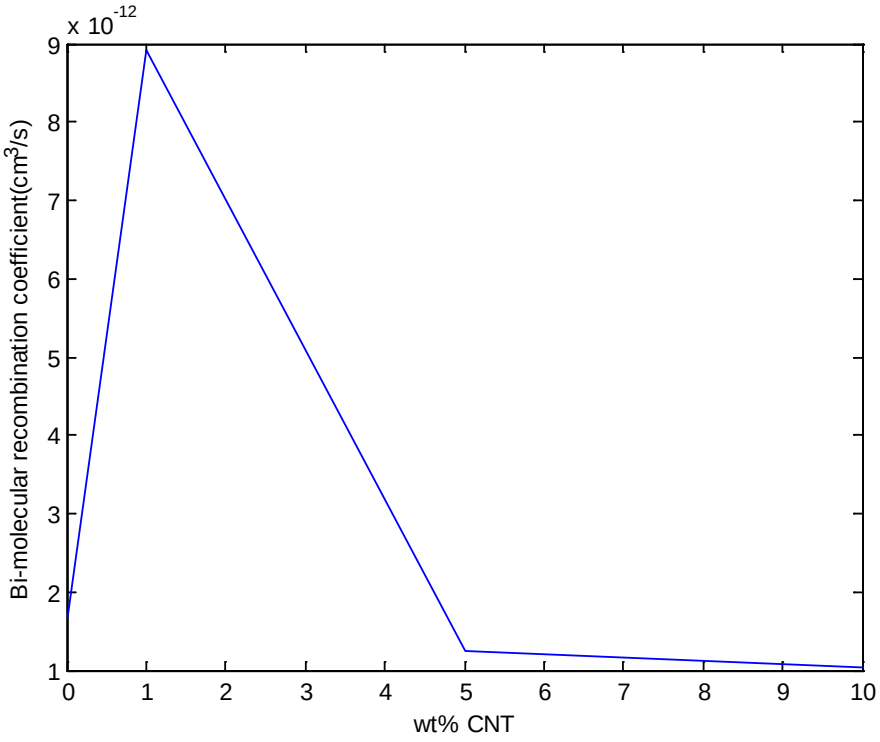

Figure 25: Change in Bi-molecular recombination coefficient with increasing weight percentage of CNT

4.4 Characteristic Performance of P3HT:PCBM

4.4.1 Effect of changing Thickness on Short Circuit Current Density of Bilayer solar cell

Figure 26 shows the variation of Shot circuit current(J_{sc}) for P3HTPCBM with the varying thickness of the active layer. In the figure the maximum J_{sc} at 80nm is (3.5181). Further increase in thickness current density decreased.

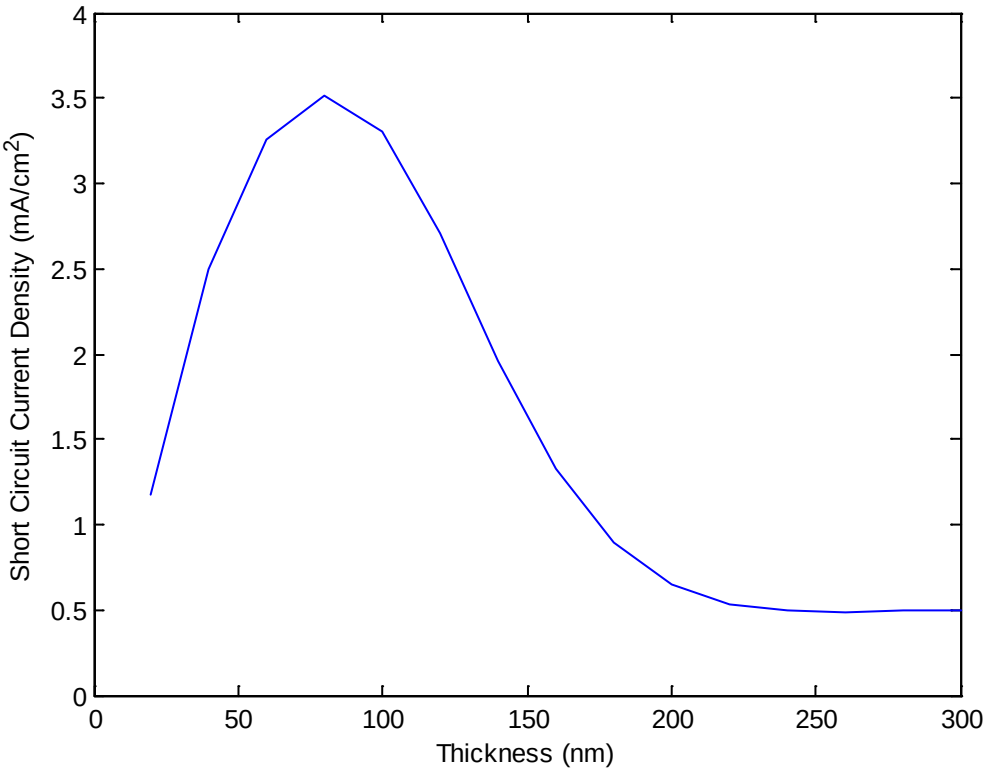

Figure 26: Change in J_{sc} with increasing Active layer thickness of P_3HT:PCBM

4.4.2 Effect of changing Thickness on Open Circuit Voltage of Bilayer solar cell

Figure 27 shows the variation of open circuit voltage(V_{oc}) for P3HT:PCBM with the varying thickness of the active layer. In the figure the V_{oc} remained the same because in our modeling we kept the photon absorption rate and energy levels constant.

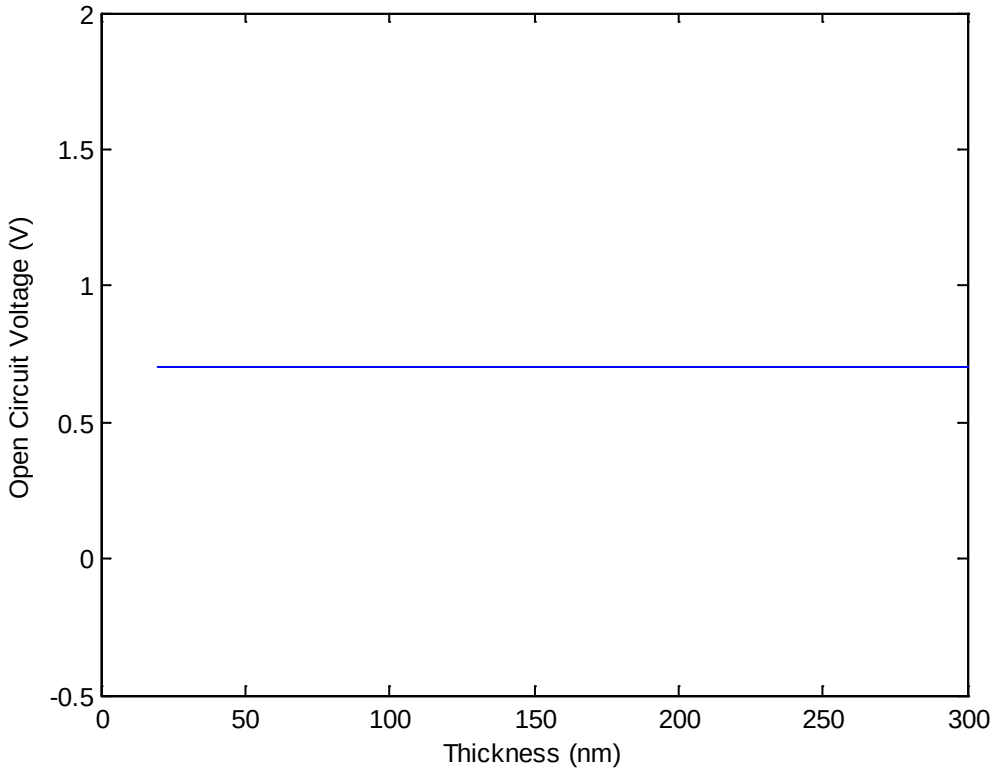

Figure 27: Change in V_{oc} with increasing Active layer thickness of P_3HT:PCBM

4.4.3 Effect of changing Thickness on Fill Factor of Bilayer solar cell

Figure 28 shows the variation of Fill Factor(FF) for P3HT:PCBM with the varying thickness of the active layer. In the figure the maximum FF at 80nm is (0.93348). Further increase in thickness Fill Factor decreases.

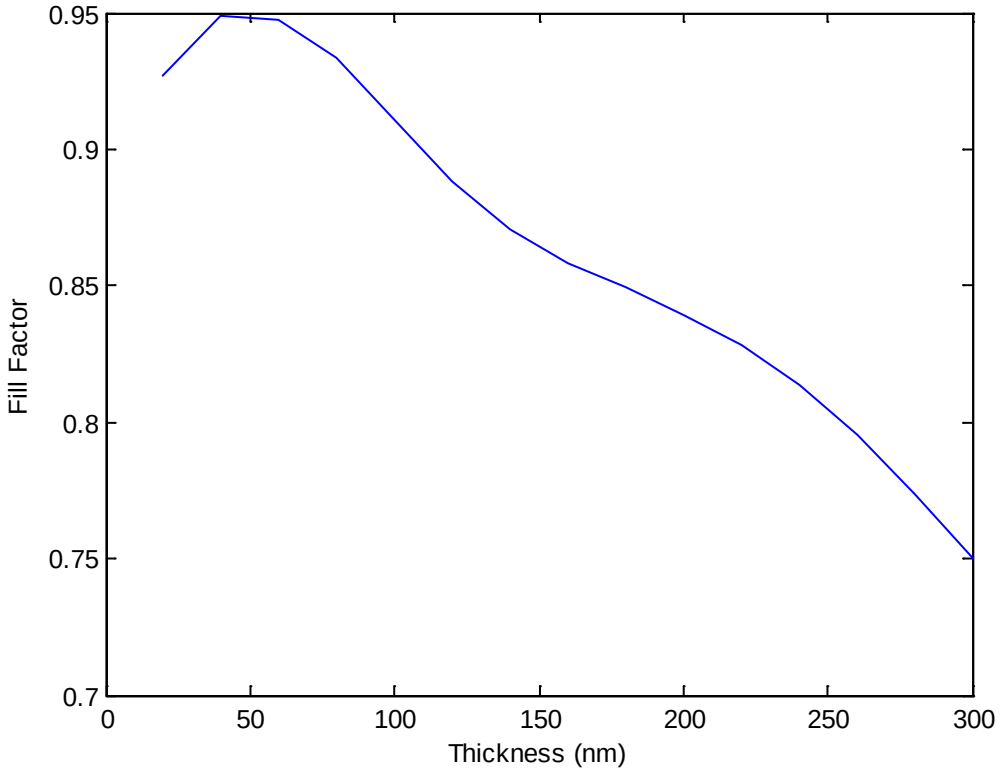

Figure 28: Change in Fill Factor(FF) with increasing Active layer thickness of P_3HT:PCBM

4.4.4 Effect of changing Thickness on Efficiency of Bilayer solar cell

Figure 29 shows the variation of efficiency for P3HT:PCBM with the varying thickness of the active layer. In the figure the maximum FF at 80nm is (2.2989). Further increase in thickness Efficiency decreases.

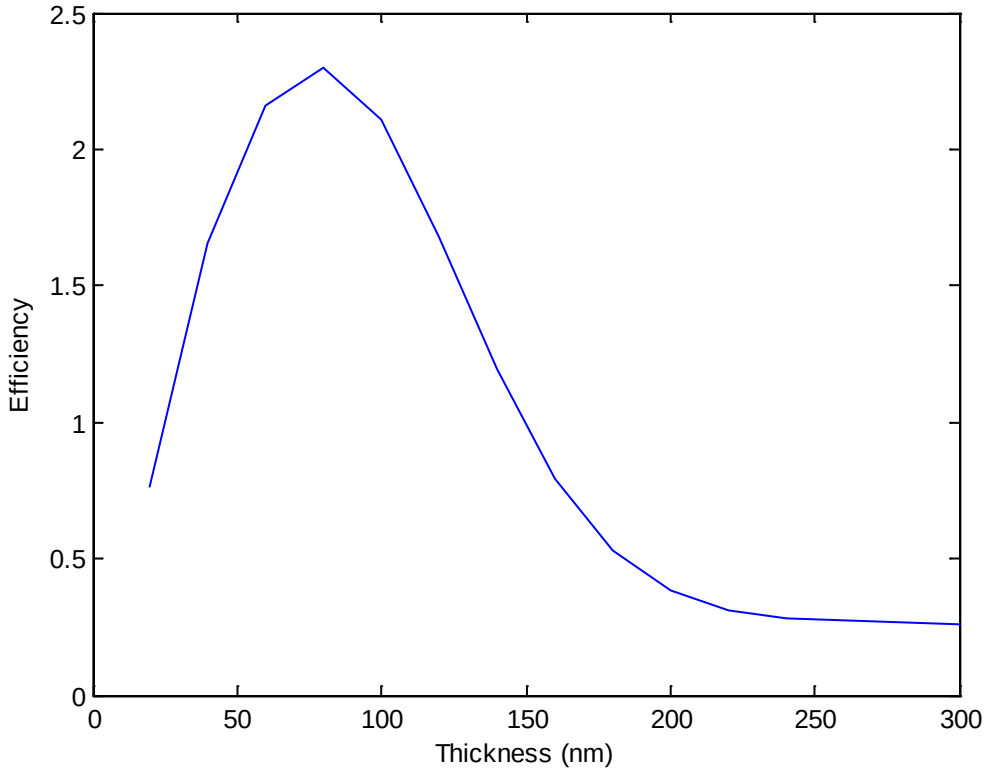

Figure 29: Change in Efficiency with increasing Active layer thickness of P_3HT:PCBM

4.5 Electrical Analysis of CNT based Bilayer Solar Cells

4.5.1 J-V Characteristic of P_3HT:CNT:PCBM based bilayer solar Cell

The photovoltaic performance of P3HT:CNT:PCBM based planar heterojunction solar cell devices were simulated using the model explained at section 3.1. Figure 30 shows the J-V characteristics of solar cells achieved by varying concentration of CNT's. The solar cell parameters obtained from Figure 30 is summarized in table 2.

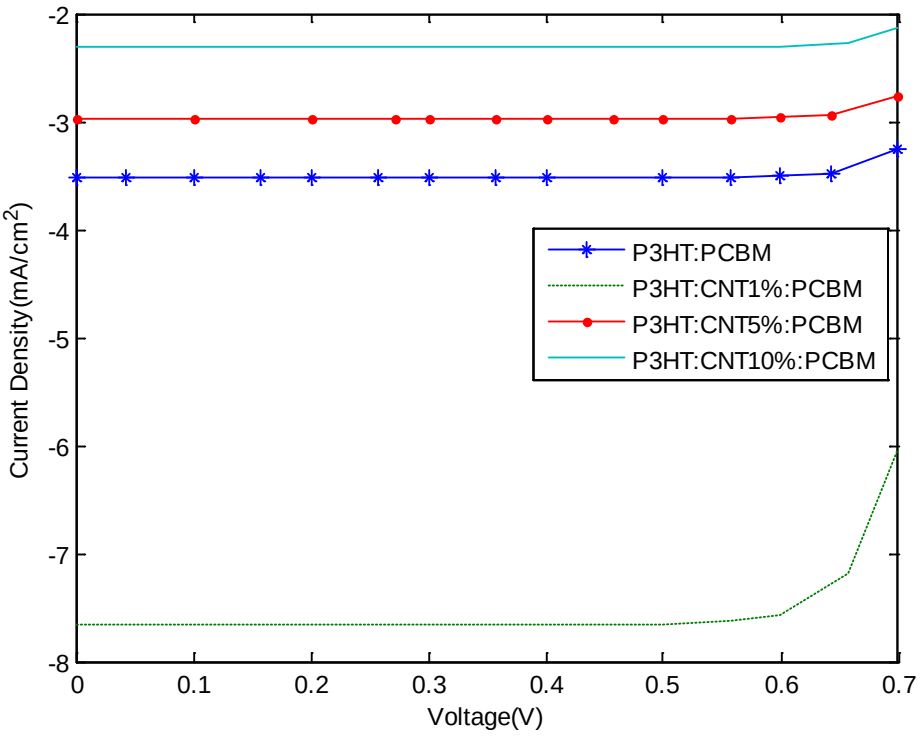

Figure 30: J-V Characteristic of P_3HT:CNT:PCBM based bilayer solar cell

% of CNT in P_3HT	J_{sc}(mA/cm^2)	V_{oc}(V)	FF	PCE (%)
0	3.5181	0.7	0.93348	2.2989
1	7.6548	0.7	0.80085	4.7221
5	2.9691	0.7	0.93531	1.9439
10	2.3102	0.7	0.93191	1.507

Table 2: Photovoltaic parameters of P_3HT:CNT:PCBM solar cells

4.5.2 Effect of adding CNT on the thickness optimized Short Circuit Current Density of Bilayer solar cell

The highest value of J_{sc} (7.6584 mA/cm^2) was obtained at 1 weight percentage CNT, which was 117% greater than the J_{sc} (3.5181 mA/cm^2) of the reference device. For CNT concentrations greater than 1weight percentage, J_{sc} remained higher than that of the reference device but was significantly lower than that of the optimized device (1wt %). The enhancement in J_{sc} at low concentrations (1wt %) of CNT is mainly due to the increase in diffusion length which enhanced due to the higher mobility of SWCNTs. the lowering of the J_{sc} for further addition SWCNTs could be attributed to the fact that the effective hole mobility of the polymer composted for higher ratio of SWCNT(weight percentage >1%) decreases.

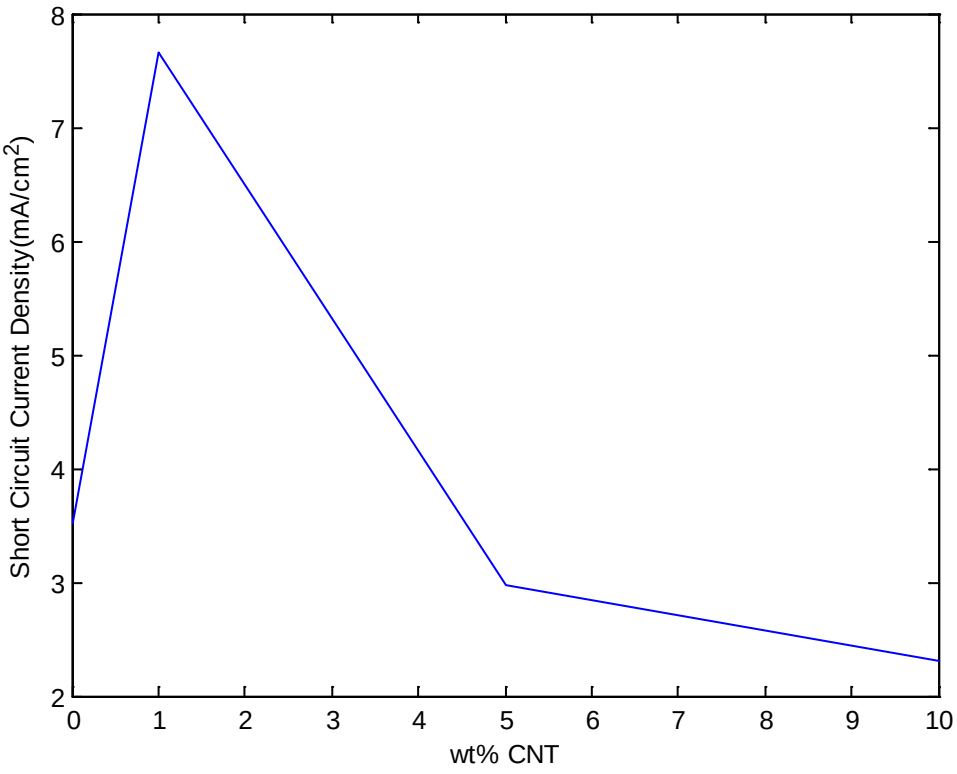

Figure 31: Change in short circuit current density with increasing weight percentage of CNT

4.5.3 Effect of adding CNT on the thickness optimized Open Circuit Voltage of Bilayer solar cell

V_{oc} is actually a factor of the exciton generation rate and the energy levels of the acceptor and donor. Since both the parameters of the low weight percentage P_3HT:CNT:PCBM are assumed to be constant, the V_{oc} remains the same .

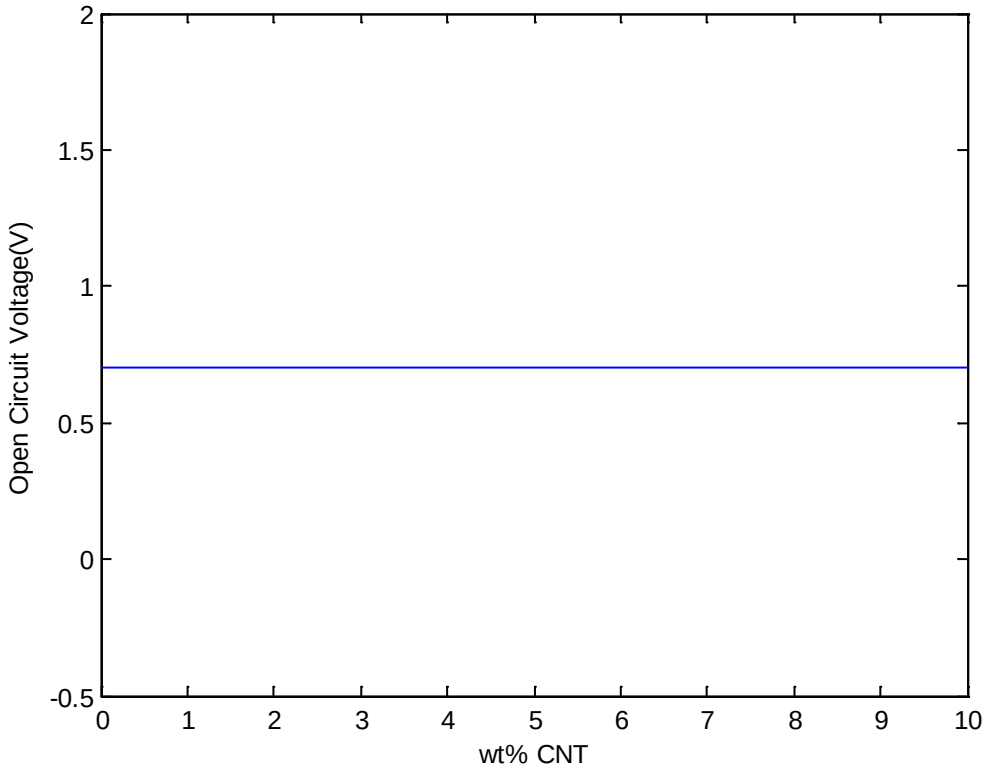

Figure 32: Change in open circuit voltage with increasing weight percentage of CNT

4.5.4 Effect of adding CNT on the thickness optimized Fill Factor of Bilayer solar cell

Figure 33 shows the Fill Factor (FF) with increasing CNT weight percentage. Highest fill factor (0.9351) was obtained at 5weight percentage concentration. In our figure at 0weight percentage the fill factor was (0.93348) and then further addition of CNT in the active layer composite it decreases to (0.88085) at 1weight percentage. Then further addition of CNT it rises to max at 5 weight percentage. FF is a function of multiple parameters, thus the improvement in FF at 5weight percentage CNT cannot be attributed to a single factor. Since FF is primarily a function of maximum power (P_{max}) and carrier mobility, the main reasons for the improvement in FF at 1weight percentageCNT could be attributed to the improvement in P_{max} and effective hole mobility.

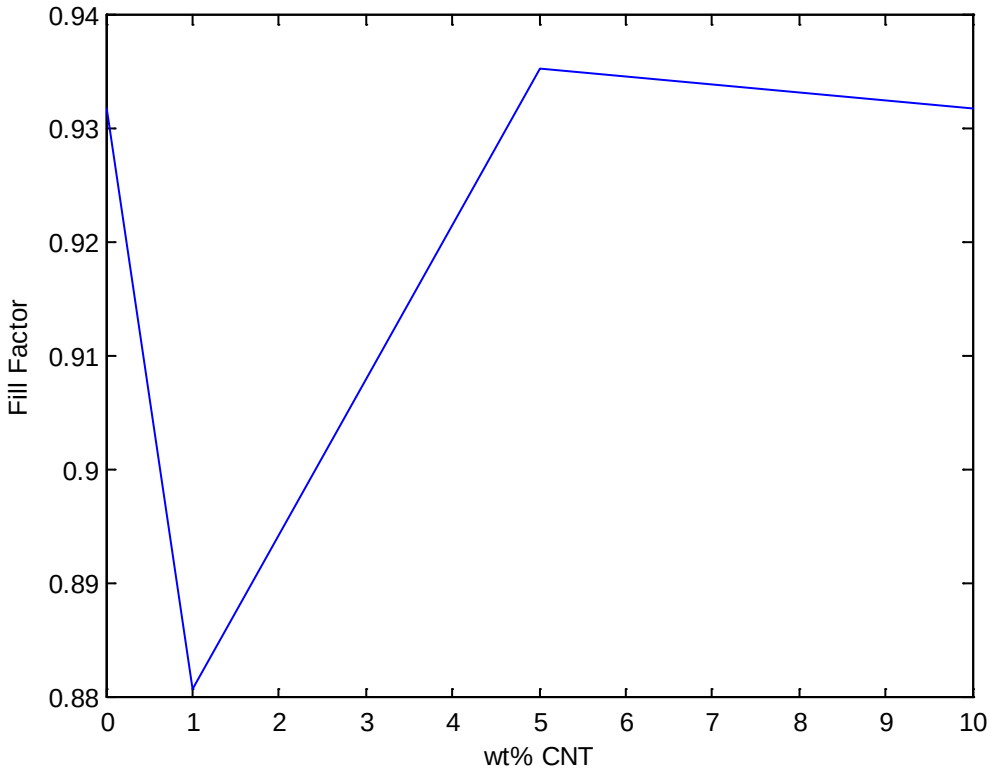

Figure 33: Change in fill-factor with increasing weight percentage of CNT

4.5.5 Effect of adding CNT on the thickness optimized Efficiency of Bilayer solar cell

Figure 34 shows the change in power conversion efficiency with increasing weight percentage of CNT The addition of 1weight percentage CNT to the active layer improved the PCE from 2.2989 (reference device) to 4.7221 which corresponds to a 105% enhancement in PCE, further increase in the content of CNT resulted in lowering of the efficiencies. The PCE improved primarily due to the improvement of the J_{sc}.

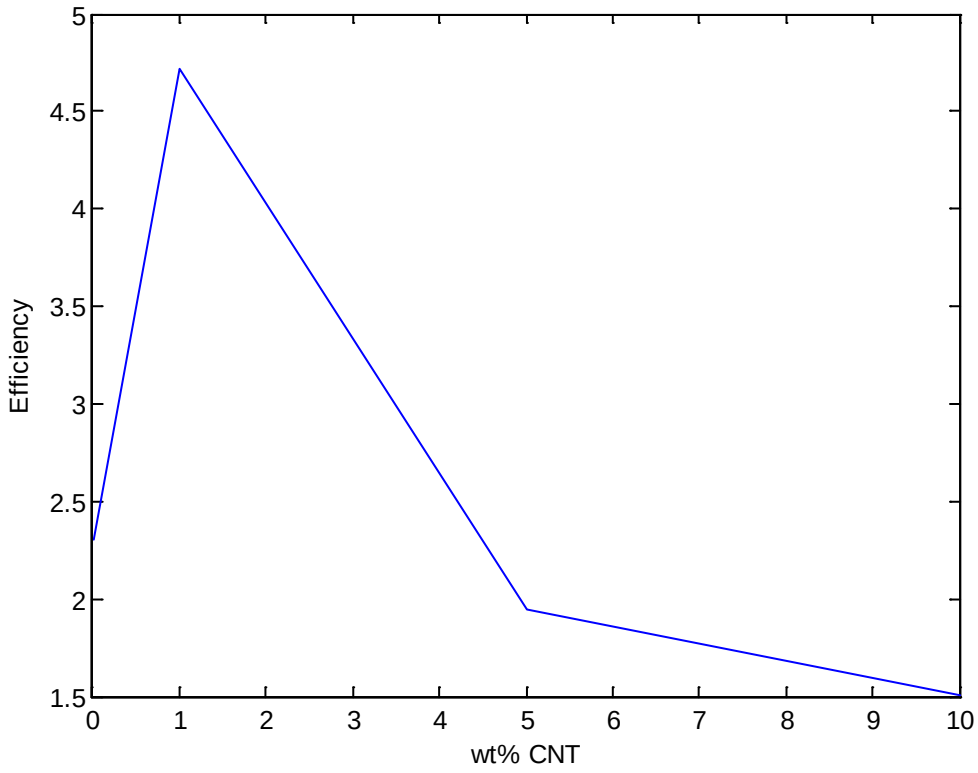

Figure 34: Change in Power conversion efficiency with increasing weight percentage of CNT

4.6 Effect of adding CNT on the Characteristic Performance of Bilayer solar cell

4.6.1 Effect of changing CNT weight percentage on Short Circuit Current Density of Bilayer solar cell

The figure 35 show the Shot Circuit current (J_{sc}) after adding CNT of different weight percentage. The figure shows the maximum current density of (7.6584) at 80nm adding 1weight percentage. Then further increase in the weight percentage to 5,10 the Current density decreases.

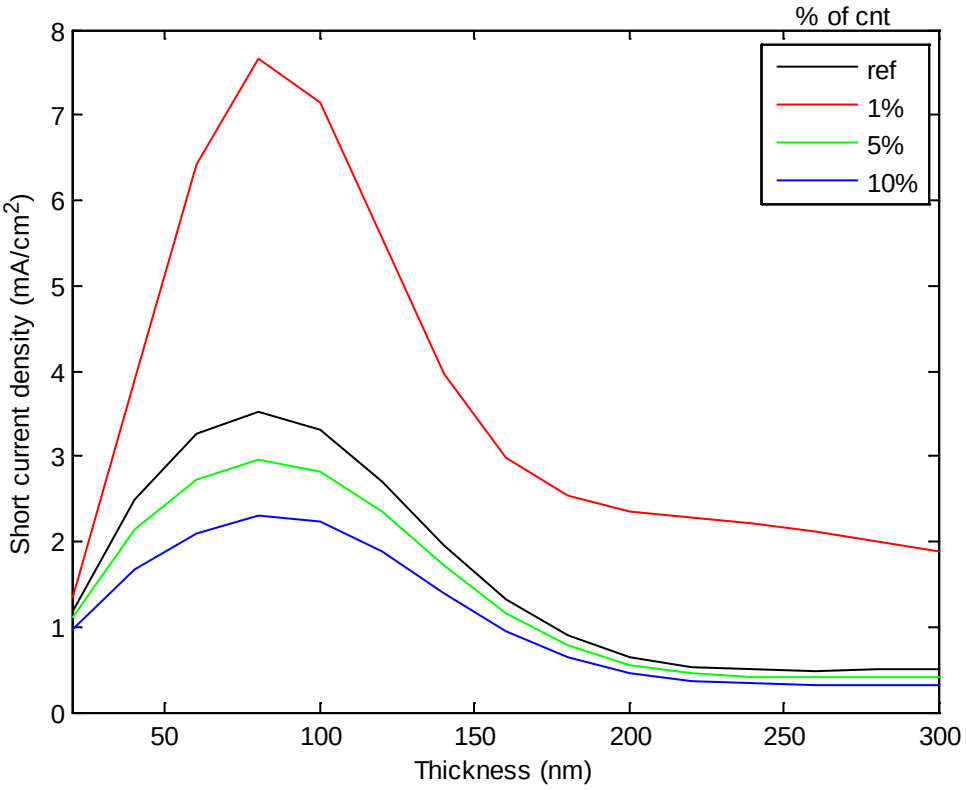

Figure 35: Change in J_{sc} with increasing Active layer thickness of P_3HT:CNT:PCBM

4.6.2 Effect of changing CNT weight percentage on Fill Factor of Bilayer solar cell

The figure 36 show the Fill Factor after adding CNT of different weight percentage. The figure shows the maximum Fill factor of (0.95057) at 60nm adding 5weight percentage. Then at 1 weight percentage the fill factor came out to be (0.90334) at 40nm. The fill factor depends on many factor, therefore we need to improve the fill factor at 1weight percentage.

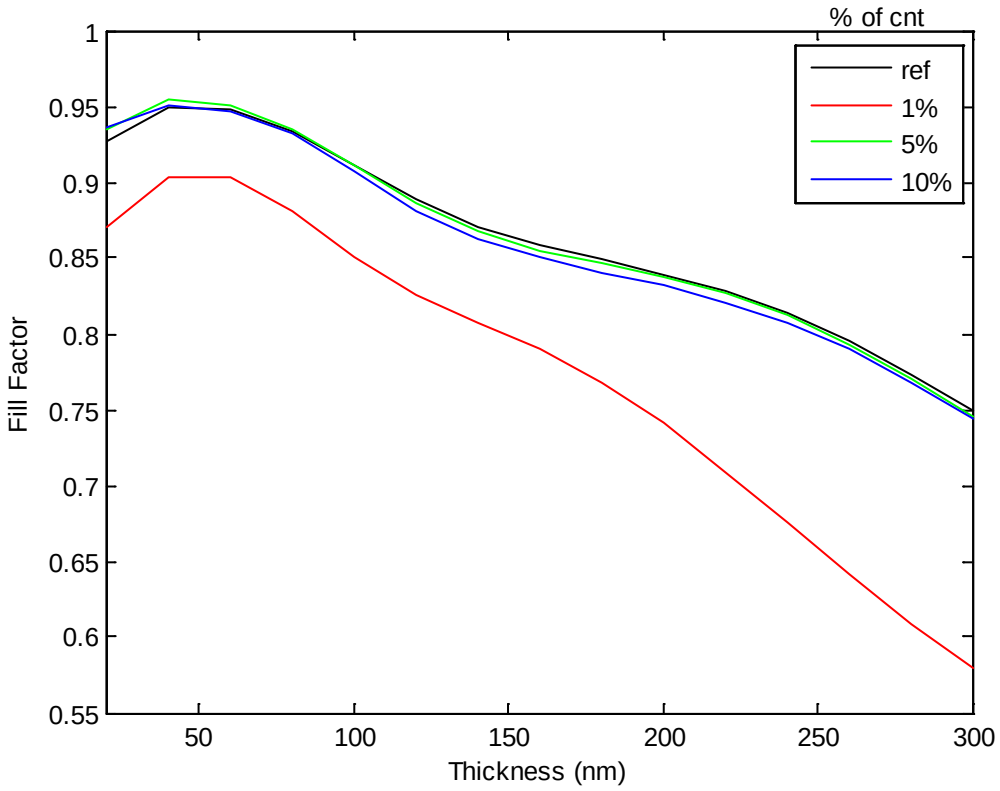

Figure 36: Change in Fill Factor with increasing Active layer thickness of P_3HT:CNT:PCBM

4.6.3 Effect of changing CNT weight percentage on Efficiency of Bilayer solar cell

The figure 37 show the Efficiency after adding CNT of different weight percentage. The figure shows the maximum efficiency of (4.7221) at 80nm adding 1weight percentage. Then further increase in the weight percentage to 5,10 the efficiency decreases.

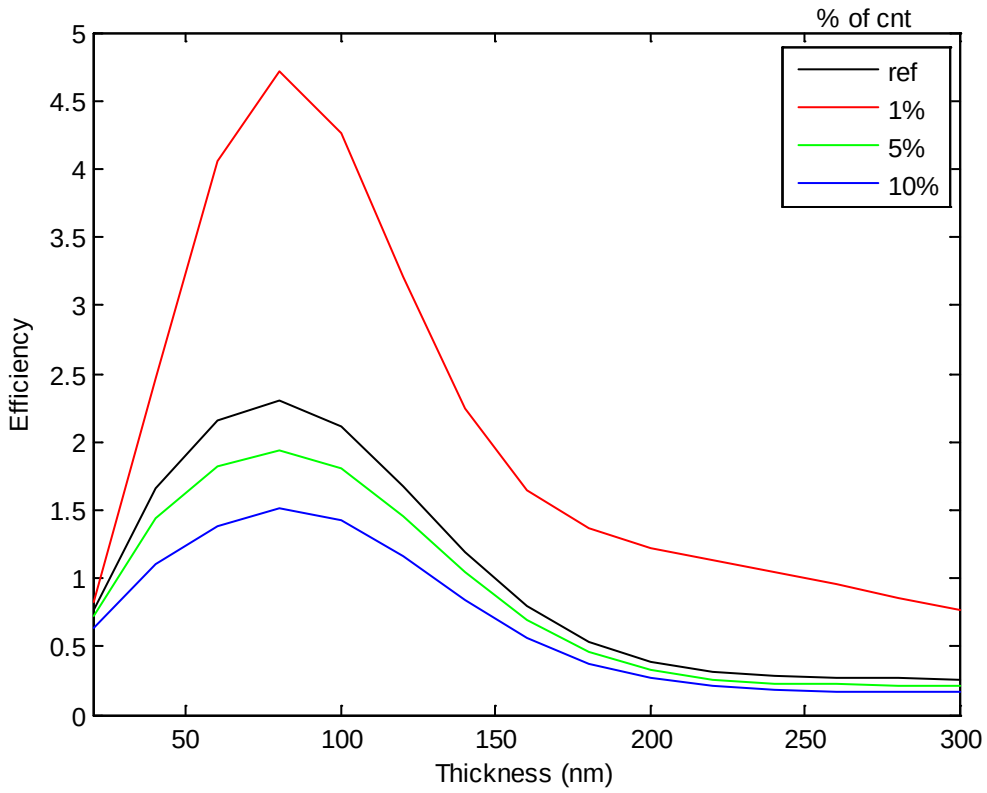

Figure 37: Change in Efficiency with increasing Active layer thickness of P_3HT:CNT:PCBM

5. CONCLUSION AND FUTURE WORK

5.1 CONCLUSION

In the conclusion the performance ofP_3HT:CNT:PCBM based Bilayer solar cell was simulated. The reference solar cell device with an active layer composed of P_3HT:PCBM was found to have a short circuit current density (J_{sc}) of 3.5181 mA, an open circuit voltage (V_{oc}) of 0.7 V and a fill factor (FF) of 0.93348 leading to a PCE of 2.2989. The highest PCE was achieved through the incorporation at 1weight percentageCNT. Upon the addition of 1weight percentageCNT the J_{sc}, V_{oc} and FF enhanced to 7.6584mA, 0.7V and 0.88085 leading to an improved PCE of 4.7221. Incorporation of CNTs above 1% resulted decreased the PCE. J-V analysis revealed that the solar cell parameters limiting the PCE at higher weight percentage of CNT was the FF and J_{sc}. From our theoretical analysis we found that the decrease inJ_{sc} and FF for higher weight percentage of CNT was due the decrease in effective hole mobility at higher concentrations of CNT. The decrease in effective hole mobility was attributed to the presence of CNT which made a pathway for EHP recombination and CNT aggregation which decreased the dissociation probability. We then predicted the J-V characteristics of 80 nm thick P_3HT:CNT:PCBM based bilayer solar cells by considering CNTs without any impurities.

5.2 FUTURE WORK

Further improvement in the PCE of a Bilayer solar cell could be achieved by simulating the effect of adding:

- Low band gap polymer (PTB_7) with greater hole carrier mobility
- Higher absorbing PC_{70}BM with greater electron mobility
- Hole Transport Layer
- CNTS of different chiralities and diameter

References

1. *IPCC Second Assessment*, in *Intergovernmental Panel on Climate Change*1995.

2. Hassan, A.Y., *Islamic Technology: An illustrated history.* Donald Routledge Hill, 1986.

3. *World Wind Energy Report 2010*. World Wind Energy Association WWEA, 2011.

4. *Use and Capacity of Global Hydropower Increases*, 2012, Worldwatch Institute.

5. *Basic Research Needs for Solar Energy Utilization*, 2005, US Department of Energy.

6. Perlin, J., *From Space to Earth: The Story of Solar Electricity*. 1999.

7. *Photovoltaic Milestones: US Energy Information Administration*: http://www.eia.gov/cneaf/solar.renewables/renewable.energy.annual/backgrnd/chap11i.htm.

8. Wolden, C.A., et al., *Photovoltaic manufacturing: Present status, future prospects, and research needs.* J. Vac. Sci. Technol. A, 2011. 29(3): p. 030801.

9. *Crystalline Silicon Photovoltaics Research*, 2011, US Dept. of Energy: http://www1.eere.energy.gov/solar/sunshot/pv_crystalline_silicon.html.

10. Green, M.A., et al., *Solar cell efficiency tables (version 40).* Prog. Photovolt. Res. Appl., 2012. 20(5): p. 606-614.

11. Clarke, C., *San Jose Solar Company Breaks Efficiency Record for PV*, 2012: http://www.kcet.org/news/rewire/solar/photovoltaic-pv/san-$J_o$se-solar-company-breaks-efficiency-record-for-pv.html.

12. Gratzel, M., *Photoelectrochemical cells.* Nature, 2001. 414: p. 338-344.

13. Gratzel, M., *Solar Energy Conversion by Dye-Sensitized Photovoltaic Cells.* Inorg. Chem., 2005. 44.

14. Yella, A., et al., *Porphyrin-Sensitized Solar Cells with Cobalt (II/III)–Based Redox Electrolyte Exceed 12 Percent Efficiency.* Science, 2011. 334(6056): p. 629-634.

15. Ip, A.H., et al., *Hybrid passivated colloidal quantum dot solids.* Nature Nanotechnology, 2012. 7: p. 577-582.

16. Sariciftci, N.S., et al., Appl. Phys. Lett., 1993. 62.

17. Karg, S., et al., *Electrical and optical characterization of poly(phenylene-vinylene) light emitting diodes.* Synth. Met., 1993. 54(1-3).

18. Marks, R.N., et al., J. Phys. Condens. Mater. 1994. 6.

19. Yu, G., et al., *Polymer Photovoltaic Cells: Enhanced Efficiencies via a Network of Internal Donor-Acceptor Heterojunctions.* Science, 1995. 270.

20. Halls, J.J.M., et al., Nature, 1995. 376.

21. Hoppe, H. and N.S. Sariciftci, *Organic solar cells: An overview.* $J_o$urnal of Materials Research, 2004. 19(7): p. 1924-1945.

22. Brabec, C.J., N.S. Sariciftci, and J.C. Hummelen, *Plastic Solar Cells.* Advanced Functional Materials, 2001. 11(1): p. 15-26.

23. Spanggaard, H. and F.C. Krebs, *A brief history of the development of organic and polymeric photovoltaics.* Solar Energy Materials and Solar Cells, 2004. 83(2-3): p. 125-146.

24. News, H. *Heliatek consolidates its technology leadership by establishing a new world record for organic solar technology with a cell efficiency of 12%.* 2013.

25. Yoo, S., B. Domercq, and B. Kippelen, *Intensity-dependent equivalent circuit parameters of organic solar cells based on pentacene and C [sub 60].* $J_o$urnal of Applied Physics, 2005. 97(10): p. 103706.

26. Potscavage, W.J., et al., *Encapsulation of pentacene/*C_{60} *organic solar cells with Al2O3 deposited by atomic layer deposition.* Applied Physics Letters, 2007. 90(25): p. 253511.

27. Yang, J. and T.-Q. Nguyen, *Effects of thin film processing on pentacene/*C_{60} *bilayer solar cell performance.* Organic Electronics, 2007. 8(5): p. 566-574.

28. Sullivan, P. and T. $J_o$nes, *Pentacene/fullerene (*C_{60}*) heterojunction solar cells: Device performance and degradation mechanisms.* Organic Electronics, 2008. 9(5): p. 656-660.

29. Niggemann, M., et al., *Light trapping in organic solar cells* physica status solidi, 2008. 205(12): p. 2862–2874.

30. Mott, N.F. *Note on the contact between a metal and an insulator or semiconductor*. in *Proc. Cambr. Phil. Soc.* 1938.

31. monch, W., *Metal-semiconductor contacts: electronic properties.* Surface Science, 1994. 299/300: p. 928-944.

32. Greenham, N.C. and R.H. Friend, *Semiconductor device physics of conjugated polymers.* Solid State Physics, 1995. 49(1).

33. Chen, L.-M., et al., *Interface investigation and engineering – achieving high performance polymer photovoltaic devices. J$_o$*urnal of Materials Chemistry, 2010. 20(13): p. 2575.

34. Mihailetchi, V.D., et al., *Cathode dependence of the open-circuit voltage of polymer:fullerene bulk heterojunction solar cells.* Journal of Applied Physics, 2003. 94(10).

35. Brabec, C.J., et al., *Origin of the Open Circuit Voltage of Plastic Solar Cells.* Adv Funct. Mater, 2001. 11(5): p. 374-380.

36. Crispin, X., *Interface dipole at organic/metal interfaces and organic solar cells.* Solar Energy Materials and Solar Cells, 2004. 83: p. 147-168.

37. Kumar, A., S. Sista, and Y. Yang, *Dipole induced anomalous S-shape I-V curves in polymer solar cells. J$_o$*urnal of Applied Physics, 2009. 105(9): p. 094512.

38. Kim, J.Y., et al., *New Architecture for High-Efficiency Polymer Photovoltaic Cells Using Solution-Based Titanium Oxide as an Optical Spacer.* Advanced Materials, 2006. 18(5): p. 572-576.

39. Wu, S., et al., *pH-neutral PEDOT:PSS as hole injection layer in polymer light* Organic Electronics, 2011. 12(3): p. 504-508.

40. Koch, N., A. Elschner, and R.L. *J$_o$*hnson, *Green polyfluorene-conducting polymer interfaces: Energy level alignment and device performance.* J. Appl. Phy., 2006. 100(2).

41. Zhang, F.L., et al., *Influence of buffer layers on the performance of polymer solar cells.* Appl. Phys. Lett., 2004. 84(19): p. 3906-3908.

42. Kim, Y., et al., *Effects of thickness and thermal annealing of the PEDOT:PSS layer on the performance of polymer solar cells.* Organic Electronics, 2009. 10(1): p. 205-209.

43. Kim, Y.-H., et al., *Performance and stability of electroluminescent device with self-assembled layers of poly(3,4-ethylenedioxythiophene)–poly(styrenesulfonate) and polyelectrolytes.* Thin Solid Films, 2006. 510(1-2): p. 305-310.

44. Jong, M.P.d., L.J.v. IJzendoorn, and M.J.A.d. Voigt, *Stability of the interface between indium-tin-oxide and poly(3,4-ethylenedioxythiophene)/poly(styrenesulfonate) in polymer light-emitting diodes.* Appl. Phys. Lett., 2000. 77(14): p. 2255-2257.

45. Cruz-Cruz, et al., *Study of the effect of DMSO concentration on the thickness of the PSS insulating barrier in PEDOT:PSS thin films.* Synth. Met., 2010. 160(13-14): p. 1501-1506.

46. Ouyang, J., et al., *On the mechanism of conductivity enhancement in poly(3,4-ethylenedioxythiophene):poly(styrene sulfonate) film through solvent treatment.* Polymer, 2004. 45: p. 8443-8450.

47. Zhang, C., et al., *Inverted Organic Photovoltaic Cells with Solution-Processed Zinc Oxide as Electron Collecting Layer.* Japanese $J_o$urnal of Applied Physics, 2011. 50(8): p. 082302

.

48. Dou, L., et al., *Tandem Polymer Solar Cells Featuring a Spectrally Matched Low-Bandgap Polymer.* Nature Photonics, 2012. 6: p. 180-185.

49. Kim, D.Y., et al., *The effect of molybdenum oxide interlayer on organic photovoltaic cells.* Appl. Phys. Lett., 2009. 95.

50. Shrotriya, V., et al., *Transition metal oxides as the buffer layer for polymer photovoltaic cells.* Appl. Phys. Lett., 2006. 88(7).

51. Lögdlund, M. and J.L. Brédas, *Theoretical studies of the interaction between aluminum and poly(p-phenylenevinylene) and derivatives.* J. Chem. Phy., 1994. 101(5): p. 4357-4364.

52. Antoniadis, H., et al., *Photovoltaic and photoconductive properties of aluminum/poly(p-phenylene vinylene) interfaces.* Synth. Met., 1994. 62(3): p. 265-271.

53. Gupta, D., M. Bag, and K.S. Narayan, *Correlating reduced fill factor in polymer solar cells to contact effects.* Applied Physics Letters, 2008. 92(9): p. 093301.

54. Huang, J., Z. Xu, and Y. Yang, *Low-Work-Function Surface Formed by Solution-Processed and Thermally Deposited Nanoscale Layers of Cesium Carbonate.* Adv. Funct. Mater., 2007. 17: p. 1966-1973.

55. Shaheen, S.E., et al., *Bright blue organic light-emitting diode with improved color purity using a LiF/Al cathode.* J. Appl. Phy., 1998. 84(4): p. 2324-2327.

56. Hung, L.S., C.W. Tang, and M.G. Mason, *Enhanced electron injection in organic electroluminescence devices using an Al/LiF electrode.* Appl. Phys. Lett., 1997. 70(2): p. 152-154.

57. Brabec, C.J., et al., *Effect of LiF/metal electrodes on the performance of plastic solar cells.* Appl. Phys. Lett., 2002. 80(7): p. 1288-1290.

58. Huang, J., et al., *Improving the power efficiency of white light-emitting diode by doping electron transport material.* Applied Physics Letters, 2006. 89(13): p. 133509.

59. Huang, J., et al., *Achieving High-Efficiency Polymer White-Light-Emitting Devices.* Adv. Mater., 2006. 18: p. 114-117.

60. Huang, J., et al., *Detailed analysis of bathocuproine layer for organic solar cells based on copper phthalocyanine and* C_{60}. J. Appl. Phy., 2009. 105.

61. Gommans, H., et al., *On the Role of Bathocuproine in Organic Photovoltaic Cells.* Advanced Functional Materials, 2008. 18(22): p. 3686-3691.

62. Hayakawa, A., et al., *High performance polythiophene/fullerene bulk-heterojunction solar cell with a TiOx hole blocking layer.* Applied Physics Letters, 2007. 90(16): p. 163517.

63. Yoshikawa, O., et al., *Enhanced Efficiency and Stability in* P_3HT*:PCBM Bulk Heterojunction Solar Cell by using* TiO_2 *Hole Blocking Layer.* Material Research Society, 2007. 965.

64. Manor, A., et al., *Enhancing functionality of ZnO hole blocking layer in organic photovoltaics.* Solar Energy Materials and Solar Cells, 2012. 98: p. 491-493.

65. Hau, S.K., et al., *Air-stable inverted flexible polymer solar cells using zinc oxide nanoparticles as an electron selective layer.* Applied Physics Letters, 2008. 92(25): p. 253301.

66. Michaelson, H.B., *The work function of the elements and its periodicity.* J. Appl. Phy., 1977. 48(11): p. 4729-4733.

67. Mihailetchi, V.D., L.J.A. Koster, and P.W.M. Blom, *Effect of metal electrodes on the performance of polymer:fullerene bulk heterojunction solar cells.* Appl. Phys. Lett., 2004. 85(6): p. 970-972.

68. Ishii, H., et al., *Kelvin probe study of band bending at organic semiconductor/metal interfaces: examination of Fermi level alignment.* phys. stat. sol.(a), 2004. 201(6): p. 1075-1094.

69. Rajaputra, S., S. Vallurupalli, and V.P. Singh, *Schottky diode solar cells on electrodeposited copper phthalocyanine films.* Sol. Energy Mater. Sol. Cells, 2009. 93(1): p. 60-64.

70. Kwong, C.Y., et al., *Improvement of the efficiency of phthalocyanine organic Schottky solar cells with ITO electrode treatment.* Appl. Phys. A, 2003. 77: p. 555-560.

71. Jiangeng Xue, S.U., Barry P Rand, Stephen R Forrest, *4.2% efficient organic photovoltaic cells with low series resistances.* Appl. Phys. Lett., 2004. 84(16): p. 3013-3015.

72. Peumans, P. and S.R. Forrest, *Very-high-efficiency double-heterostructure copper phthalocyanine/C_{60} photovoltaic cells.* Appl. Phys. Lett., 2001. 79(1): p. 126-128.

73. Shaw, P.E., A. Ruseckas, and I.D.W. Samuel, *Exciton Diffusion Measurements in Poly(3-hexylthiophene).* Adv Mater, 2008. 20(18): p. 3516-3520

74. Rockett, A., *Organic Semiconductors*, in *The Materials Science of Semiconductors*. 2008, Springer US. p. 395-453.

75. Gregg, B.A., S.-G. Chen, and R.A. Cormier, *Coulomb Forces and Doping in Organic Semiconductors.* Chem. Mater., 2004. 16(23): p. 4586-4599.

76. Horowitz, G., *Organic Field-Effect Transistors.* Adv Mater, 1998. 10(5): p. 365-377.

77. Deibel, C. and V. Dyakonov, *Polymer–fullerene bulk heterojunction solar cells.* Reports on Progress in Physics, 2010. 73(9): p. 096401.

78. Cheyns, D., et al., *Analytical model for the open-circuit voltage and its associated resistance in organic planar heterojunction solar cells.* Physical Review B, 2008. 77(16).

79. Koster, L.J.A., et al., *Light intensity dependence of open-circuit voltage of polymer:fullerene solar cells.* Applied Physics Letters, 2005. 86(12): p. 123509.

80. Scharber, M.C., et al., *Design Rules for Donors in Bulk-Heterojunction Solar Cells—Towards 10 % Energy-Conversion Efficiency.* Advanced Materials, 2006. 18(6): p. 789-794.

81. Shockley, W. and H.J. Queisser, *Detailed Balance Limit of Efficiency of p-n Junction Solar Cells.* J. Appl. Phy., 1961. 32(3): p. 510-519.